

This is a repository copy of *Isotopic compositions, nitrogen functional chemistry, and low-loss electron spectroscopy of complex organic aggregates at the nanometer scale in the carbonaceous chondrite Renazzo*.

White Rose Research Online URL for this paper:  
<https://eprints.whiterose.ac.uk/152268/>

Version: Published Version

---

**Article:**

Vollmer, Christian, Leitner, Jan, Kepaptsoglou, Demie [orcid.org/0000-0003-0499-0470](https://orcid.org/0000-0003-0499-0470) et al. (3 more authors) (2019) Isotopic compositions, nitrogen functional chemistry, and low-loss electron spectroscopy of complex organic aggregates at the nanometer scale in the carbonaceous chondrite Renazzo. *Meteoritics & planetary science*. ISSN 1086-9379

<https://doi.org/10.1111/maps.13389>

---



**Reuse**

This article is distributed under the terms of the Creative Commons Attribution-NonCommercial-NoDerivs (CC BY-NC-ND) licence. This licence only allows you to download this work and share it with others as long as you credit the authors, but you can't change the article in any way or use it commercially. More information and the full terms of the licence here: <https://creativecommons.org/licenses/>

**Takedown**

If you consider content in White Rose Research Online to be in breach of UK law, please notify us by emailing [eprints@whiterose.ac.uk](mailto:eprints@whiterose.ac.uk) including the URL of the record and the reason for the withdrawal request.

## Isotopic compositions, nitrogen functional chemistry, and low-loss electron spectroscopy of complex organic aggregates at the nanometer scale in the carbonaceous chondrite Renazzo

Christian VOLLMER <sup>1\*</sup>, Jan LEITNER <sup>2</sup>, Demie KEPAPTSOGLU<sup>3,4</sup>, Quentin M. RAMASSE<sup>3,5</sup>, Henner BUSEMANN<sup>6</sup>, and Peter HOPPE<sup>2</sup>

<sup>1</sup>Institut für Mineralogie, Westfälische Wilhelms-Universität, Corrensstr. 24, 48149 Münster, Germany

<sup>2</sup>Particle Chemistry Department, Max Planck Institute for Chemistry, Hahn-Meitner-Weg 1, 55128 Mainz, Germany

<sup>3</sup>SuperSTEM Laboratory, Keckwick Lane, Daresbury, UK

<sup>4</sup>Department of Physics, Jeol Nanocentre, University of York, Heslington YO10 5DD, UK

<sup>5</sup>School of Chemical and Process Engineering, School of Physics, University of Leeds, Leeds LS2 9JT, UK

<sup>6</sup>Institut für Geochemie und Petrologie, ETH Zürich, Clausiusstr. 25, Zürich, Switzerland

\*Corresponding author. E-mail: christian.vollmer@wwu.de

(Received 11 January 2019; revision accepted 21 August 2019)

---

**Abstract**—Organic matter (OM) was widespread in the early solar nebula and might have played an important role for the delivery of prebiotic molecules to the early Earth. We investigated the textures, isotopic compositions, and functional chemistries of organic grains in the Renazzo carbonaceous chondrite by combined high spatial resolution techniques (electron microscopy–secondary ion mass spectrometry). Morphologies are complex on a submicrometer scale, and some organics exhibit a distinct texture with alternating layers of OM and minerals. These layered organics are also characterized by heterogeneous <sup>15</sup>N isotopic abundances. Functional chemistry investigations of five focused ion beam-extracted lamellae by electron energy loss spectroscopy reveal a chemical complexity on a nanometer scale. Grains show absorption at the C-K edge at 285, 286.6, 287, and 288.6 eV due to polyaromatic hydrocarbons, different carbon-oxygen, and aliphatic bonding environments with varying intensity. The nitrogen K-edge functional chemistry of three grains is shown to be highly complex, and we see indications of amine (C-NH<sub>x</sub>) or amide (CO-NR<sub>2</sub>) chemistry as well as possible N-heterocycles and nitro groups. We also performed low-loss vibrational spectroscopy with high energy resolution and identified possible D- and G-bands known from Raman spectroscopy and/or absorption from C=C and C-O stretch modes known from infrared spectroscopy at around 0.17 and 0.2 eV energy loss. The observation of multiglobular layered organic aggregates, heterogeneous <sup>15</sup>N-anomalous compositions, and indication of NH<sub>x</sub>-(amine) functional chemistry lends support to recent ideas that <sup>15</sup>N-enriched ammonia (NH<sub>3</sub>) was a powerful agent to synthesize more complex organics in aqueous asteroidal environments.

---

### INTRODUCTION

Pristine extraterrestrial samples such as petrologic types 2–3 carbonaceous chondrites, interplanetary dust particles (IDPs), Antarctic micrometeorites (AMMs), or returned mission samples contain a few wt% or rarely up to several tens of wt% of complex carbon-bearing compounds in the form of organic matter (OM). This extraterrestrial OM has long been speculated to have

played an important role in the delivery of biorelevant molecules such as amino acids and sugars to the early Earth. The OM occurs as a complex mixture of small, soluble molecules that can be extracted from bulk meteorites by solvents (“soluble organic matter,” SOM) or as a macromolecular kerogen with highly branched aliphatic and aromatic domains and heterocycles that is insoluble in organic solvents and acids (“insoluble organic matter,” IOM; Busemann et al. 2006; Alexander

et al. 2007; Derenne and Robert 2010; Martins 2011; Pizzarello and Shock 2017). This IOM fraction usually comprises the majority of the OM (70–95 wt%, Alexander et al. 2017) in these types of samples. The bulk chemical composition of the SOM and IOM is very similar except for H/C ratios, with about 20 atom% of oxygen, and less than 5 atom% of nitrogen and sulfur and other minor elements (Schmitt-Kopplin et al. 2010; Alexander et al. 2017), but can vary slightly from chondrite to chondrite group. It is therefore possible that the two components of OM in carbonaceous chondrites can be genetically connected, for example, by alteration reactions on the parent body (Sephton et al. 2003), but this is difficult to test because of the contrasting analytical approaches that extract SOM and IOM from meteorites, which might probe different fractions of the OM as a whole. Disentangling these complex modification processes is important to our understanding of the evolution of the first prebiotic molecules in extraterrestrial environments.

Further information on the morphological and chemical makeup of OM in pristine samples has been achieved by “in situ” methods without chemical separation such as electron microscopy (scanning electron microscopy, SEM; transmission electron microscopy, TEM), synchrotron radiation techniques (X-ray absorption near-edge structure, XANES; or scanning transmission X-ray microscopy, STXM), and nanoscale secondary ion mass spectrometry (NanoSIMS; e.g., Nakamura-Messenger et al. 2006; Matrajt et al. 2012; Le Guillou et al. 2014; Vollmer et al. 2014; Vinogradoff et al. 2017; Changela et al. 2018). Such an approach provides important information on unprocessed, single grains within their petrographic context and is specifically important for extremely small samples like IDPs, micrometeorites, or returned mission samples that are not accessible by bulk extraction analysis. However, up to now, only a few chondrite or IDP samples have been investigated by such combined high spatial resolution techniques (e.g., Vollmer et al. 2014). This is partly because preparation for TEM or synchrotron analyses requires extraction of thin (on the order of ~100 nm) samples by elaborate preparation techniques such as the focused ion beam (FIB) method (e.g., Zega et al. 2007; Holzapfel et al. 2009).

Another important characteristic of extraterrestrial OM is its major element isotopic composition (D/H,  $^{13}\text{C}/^{12}\text{C}$ ,  $^{15}\text{N}/^{14}\text{N}$ ). The majority of OM is isotopically comparably “normal” and only modestly enriched in D and  $^{15}\text{N}$  with respect to the Sun or the Earth (depending on the chosen reference standard), but some regions within this OM, so-called “hotspots,” are extremely enriched in D and/or  $^{15}\text{N}$  (e.g., Busemann et al. 2006, 2009), whereas the carbon isotopic composition of the majority of the OM is close to

terrestrial. The origins of these isotopic anomalies are still not well constrained and discussed controversially, but it is usually assumed that the mere existence of a D- or  $^{15}\text{N}$ -isotopic anomaly is proof that the OM is pristine and most likely derives, for example, from an outer solar nebula rather than a heavily processed reservoir. These isotopically anomalous organic grains therefore serve as targets to analyze pristine prebiotic molecules in extraterrestrial samples.

Here we have investigated OM “in situ,” that is, within a polished thin section, of the Renazzo carbonaceous chondrite, the classifying meteorite for the CR chondrite group (provided by the Natural History Museum, Vienna). This group of meteorites is well known for its highly abundant primitive components such as presolar grains, amorphous silicates, and OM (Floss and Stadermann 2009; Le Guillou et al. 2014; Abreu 2016). We have documented the textures and morphologies of OM by SEM techniques and analyzed their C-N isotopic compositions by NanoSIMS. We also investigated their mineralogical texture and functional chemistry on a nanometer scale by electron microscopy techniques in combination with electron energy loss spectroscopy (EELS) in a state-of-the-art monochromated scanning TEM (STEM) operated at 60 kV (Krivanek et al. 2013). As this acceleration voltage is below the knock-on threshold for carbon (~80 kV), electron beam damage to the regions of interest is significantly minimized. More importantly, due to the efficient monochromation capabilities, EELS experiments at synchrotron energy resolution are achievable in the electron microscope with a subnanometer probe, including measurements in the “vibrational” regime (Krivanek et al. 2014). A lot of data on C-K edge functionality obtained by synchrotron and TEM methods already exist, so we focus here on the rarely investigated N-K edge of OM and the ultra low loss regime with sub-nm resolution obtained by STEM-EELS. By these combined high-spatial resolution techniques, we aim at a deeper understanding of the evolution and processing events of OM in diverse extraterrestrial environments such as parent body aqueous alteration.

## SAMPLES AND METHODS

### Scanning Electron Microscopy and Nanoscale Secondary Ion Mass Spectrometry

Organic matter was identified in a polished and carbon-coated meteorite thin section of the Renazzo CR2 carbonaceous chondrite by SEM on an LEO 1530 field emission gun microscope at the MPI for Chemistry in Mainz (MPIC). The meteorite thin section has been

previously sliced, embedded in epoxy, polished, and carbon coated by the meteorite working group of the Natural History Museum in Vienna by conventional methods. For energy-dispersive X-ray analysis, an Oxford X-Max 80 mm<sup>2</sup> silicon drift detector was used. The main detection signal was backscattered electron (Z) contrast using a high resolution in-lens detector, where OM can be clearly identified by its darker contrast compared to surrounding matrix. Suitable targets were then selected for C-N isotopic analysis with the NanoSIMS 50 at the MPIC, where a ~100 nm Cs<sup>+</sup> primary ion beam (~1 pA) was rastered over selected sample areas (8 × 8 μm<sup>2</sup> in size), and secondary ion images of <sup>12,13</sup>C<sup>-</sup>, <sup>12</sup>C<sup>14</sup>N<sup>-</sup>, <sup>12</sup>C<sup>15</sup>N<sup>-</sup>, and <sup>28</sup>Si<sup>-</sup> were recorded in multicollection mode. Mass resolution was sufficient (m/Δm >8000, CAMECA-definition, using a 10–90% slope at mass 26) to clearly separate <sup>13</sup>C<sup>-</sup> from <sup>12</sup>C<sup>1</sup>H<sup>-</sup>, and <sup>12</sup>C<sup>15</sup>N<sup>-</sup> from both <sup>13</sup>C<sup>14</sup>N<sup>-</sup> and <sup>11</sup>B<sup>16</sup>O<sup>-</sup>. Prior to analysis, all areas were sputtered with a high current primary beam (~20 pA) to remove the carbon coating and implant primary ions for efficient secondary ion extraction. Carbon and nitrogen isotopic ratios were normalized to a synthetic N-doped SiC standard of known C-isotopic composition (δ<sup>13</sup>C<sub>PDB</sub> = -29‰; <sup>13</sup>C/<sup>12</sup>C<sub>PDB</sub> = 0.011237) and assumed N-isotopic composition of terrestrial air (δ<sup>15</sup>N<sub>air</sub> = 0; <sup>15</sup>N/<sup>14</sup>N<sub>air</sub> = 3.676 × 10<sup>-3</sup>). Additional uncertainties for the N-isotopic ratios due to matrix effects can be estimated from the study by Zinner et al. (1989). They measured the isotopic compositions of 1-hydroxybenzotriazole hydrate (C<sub>6</sub>H<sub>5</sub>N<sub>3</sub>O•H<sub>2</sub>O) and thymine (C<sub>5</sub>N<sub>2</sub>O<sub>2</sub>H<sub>6</sub>) with known N-isotopic compositions (-12‰ and +7‰, respectively), and reproduced these by SIMS within 2‰, while a simultaneously measured graphite standard (NBS-21) had, within error limits, a terrestrial N-isotopic composition. Thus, we estimate an additional uncertainty of ~15‰ for our N-isotope measurements of the OM (of unknown composition) due to matrix effects adding to the pure Poisson error from counting statistics.

The <sup>12</sup>C<sup>14</sup>N<sup>-</sup>/<sup>12</sup>C<sup>-</sup> ratios determined for the Renazzo OM in our study have relative errors of a few per mil for small nanoglobules and typically below one per mil for the larger aggregates. However, a direct calculation of atomic N/C ratios is not feasible, due to matrix effects related to the chemical structure of the nitrogen host and type of chemical bonding. For example, Zinner et al. (1989) observed a factor of four between the <sup>12</sup>C<sup>14</sup>N<sup>-</sup>/<sup>12</sup>C<sup>-</sup> ratios of 1-hydroxybenzotriazole hydrate and thymine, despite their very similar N/C ratios of 0.5 and 0.4. For data reduction and processing, in-house software developed at the MPIC was used. In calculated color-coded isotope ratio images, isotopically anomalous hotspots can be clearly identified. Deviations of the

isotopic compositions from the respective standard ratios are reported as δ-values displaying the deviation in per mil from the standard.

### Scanning Transmission Electron Microscopy–EELS

Five electron transparent (<<100 nm for 60 kV acceleration voltage) lamellae of selected, <sup>15</sup>N-isotopically anomalous organic grains were prepared with the FIB technique using a FEI/ThermoScientific Nova 600 Nanolab Dual-Beam Workstation at the MPI for Polymer Research (MPIP) in Mainz. Exposure to high energy electrons was minimized, and the lamellae were also not documented by conventional (200 kV) TEM to avoid potential damage or contamination of the sample. Before further sample analysis, all FIB lamellae were gently heat treated in vacuum for 5 h at 140 °C to remove adsorbed water and adventitious contamination from surfaces and provide clean observation conditions. This bake-out procedure is not expected to have any effect on the FIB lamellae's intrinsic OM functional chemistry: it is meant to remove adsorbed hydrocarbons only from the surfaces of the lamellae. The possible effects of this bake-out step were tested in prior work (Vollmer et al. 2014) by comparing acquired EEL spectra from the same lamella at identical locations before and after this cleaning step. No difference was observed, although in the untreated case, fine structure at the C-K edge often became obscured during observation due to mobile adsorbed amorphous contamination, demonstrating that the advantages of the procedure outweigh possible disadvantages. As samples are relatively thick for 60 kV electrons, we argue that this procedure would only affect the surfaces of lamellae, if at all, and not the bulk of the sections.

For the STEM-EELS measurements, we used a dedicated aberration-corrected Nion UltraSTEM100MC—Hermes, which was operated at 60 kV in so-called “gentle” STEM conditions (low acceleration voltage to avoid knock-on damage to carbon-based material, ultra high vacuum conditions to prevent chemical etching of the sample). The instrument is equipped with a cold field emission electron source with a nominal energy spread of around 0.3 eV (as measured by the full width at half maximum of the zero loss peak) and an electron beam monochromator, which allows continuous monochromation down to ~14 meV energy spread (FWHM) by altering the position of the monochromator slit. In addition to the energy resolution improvement, adjusting the monochromator slit width also provides a useful fine control over the electron probe current without affecting any other optical parameter (currents down to ~8 pA in the most sensitive samples were used here). The microscope features an ultrastable stage,



conventional brightfield (BF) and high angle annular dark field (HAADF) detectors and a Gatan Enfium ERS energy loss spectrometer. The vacuum system allows for ultra-high-vacuum conditions near the specimen, thus preventing sample contamination through spurious carbon buildup or chemical etching due to residual gases in the column. The probe forming optics were adjusted to provide a 0.09 nm probe with a beam convergence of 30 mrad (half-angle), while a collection half-angle of 42 mrad was chosen for EELS analysis. The energy loss spectrometer was set to dispersions of 2, 50, or 300 meV per channel, depending on the required energy range. The energy resolution was set to  $\sim 0.018$  eV for the low loss spectroscopy measurements, and between  $\sim 0.15$  and 0.3 eV for core loss spectroscopy, respectively; the choice of energy resolution was adjusted depending on the particular sample, in order to achieve the best combination of signal-to-noise ratio and electron beam current. EEL spectra were acquired in Dual EELS mode, which allows for quasi-simultaneous acquisition of low and core loss energy spectra; other EELS acquisition parameters were further tailored to obtain electron doses low enough to avoid any observable beam damage. We cannot rule out possible modifications of the analyzed organics by sample preparation (FIB) or beam damage within the STEM (i.e., H loss) completely due to the strong interaction of 60 kV electrons with OM. This could have led to an apparent reduction of C-H and N-H bonding environments within acquired EEL spectra. However, we have tried to minimize these effects based on a long-standing experience handling sensitive materials. A lot of the data were acquired in monochromatic conditions, with low beam currents below 20 pA or even down to 8 pA for the ultra-high-resolution vibrational measurements. We systematically acquired images before, during, and after analyses, and any data with observable damage (typically, when a given area was irradiated repeatedly) were discarded. We further stress that we did not measure single data points, but spectrum images using a rastered beam with several data sets across the samples, thus spreading the electron dose across relatively large specimen areas, while avoiding areas with visible surface damage or redeposited material, which are typically more prone to beam damage. Nonrepeatable data, or data indicating beam damage (revealed, e.g., by the loss of N signal or loss of near edge fine structure in the EEL spectra) were discarded from the analysis. EEL spectra from regions of interest were energy calibrated with respect to the exact position of the ZLP and the energy offset compared to spectra from a graphite standard sample, acquired under identical conditions. The spectra were background subtracted using a decaying power-law function. To aid visualization, EEL spectra of the N-K edge were denoised

using principal component analysis using the HyperSpy platform (De la Peña et al. 2018); the denoised data are plotted with the raw data, where applicable. Respective energy loss bands were then evaluated and compared to published absorption peaks in the literature.

We note here that these high energy resolution and spatial resolution spectra are inherently noisier than related spectra obtained by XANES or STXM on much larger length scales, typically micrometer instead of the nanometer scale achieved here. Preparing meteoritic samples for STEM-EELS observations also adds to the challenge, requiring a compromise between sample integrity and the thickness requirements for low acceleration voltage and high elemental sensitivity. In the case of FIB lamella OM4, for instance, the sample was comparably thick ( $>100$  nm) for 60 kV electrons, so the signal in data from this lamella was comparably low.

## RESULTS

### Textures of Organic Aggregates

We investigated the textures of 109 organic grains (2–45  $\mu\text{m}$  in size) in the CR chondrite Renazzo by SEM techniques. The OM displays a multitude of complex morphologies (Figs. 1 and 2). It consists mostly of rounded or slightly irregular grains (sub- $\mu\text{m}$  to several  $\mu\text{m}$  in size) intermingled with or attached to other minerals (sheet silicates, refractory silicates, but also sulfides) on a micrometer scale (Fig. 1: OM152; Fig. 2: OM4). Sometimes the globular grains are aggregated to form even larger clusters (Fig. 1: OM190; Fig. 2: OM164, OM210). These complex aggregates resemble the nanoglobule clusters observed in other CR chondrites, for example, the GRA 95229 chondrite (Peeters et al. 2012) and has been described in other work on Renazzo as well (Le Guillou et al. 2014). Some of these aggregates consist of much smaller organic grains ( $\ll 100$  nm) that are diffusely distributed within the meteorite matrix (Fig. 2: OM4). In some cases, the organic aggregates occur along tiny cracks within the brecciated meteorite (Fig. 1: OM55), and in one prominent example, the OM is distributed along a huge ( $\sim 10$   $\mu\text{m}$  wide) vein consisting of very small organic grains intermingled with silicates crosscutting the matrix (Fig. 1: OM196).

One intriguing morphology of organic aggregates in Renazzo consists of strongly layered globular or irregular grains, where rounded layers of OM are attached to one another in a prominent “multiglobular” arrangement (16 grains in total, Fig. 1: OM190, Fig. 2: OM166). Alternating with these concentric organic “rinds” are sometimes layers of minerals that further strengthen the pronounced multiglobular morphology (Fig. 2: OM166) and such a

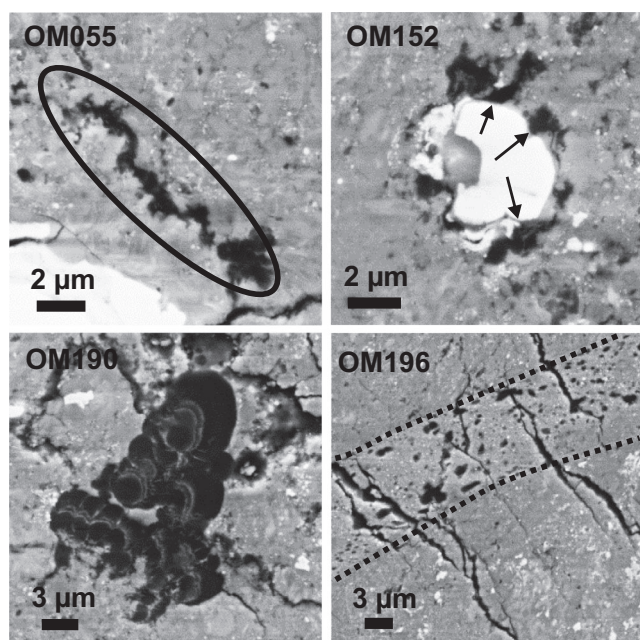


Fig. 1. Overview SEM micrographs of different OM morphologies in Renazzo. OM055) The OM fills up a crack within the fine-grained, brecciated matrix. OM152) The OM is attached to a small sulfide (troilite or pyrrhotite) grain (arrow marked). OM190) The OM is aggregated to a distinct, multiglobular texture, several microns in size. OM196) The OM occurs as micron- to submicron-sized, diffuse particles intermingled with fine-grained hydrous minerals along a huge vein clearly separated from the surrounding matrix (marked by the dashed line).

distinct “layered” texture of OM has been only rarely observed in other work (e.g., Alexander et al. 2017). In some cases, the OM is attached to distinct mineral grains such as metal, sulfides, and silicates (Fig. 1: OM152, Fig. 3: OM211).

### Isotopic Compositions of Renazzo Organics

NanoSIMS analyses of OM in Renazzo show  $^{15}\text{N}$  enrichments of up to  $\sim 2000\%$  in some of these organic aggregates, exceeding the typical  $\delta^{15}\text{N}_{\text{bulk}}$  of  $\sim 150\text{--}300\%$  for CR IOM (Alexander et al. 2007), whereas most of the  $\delta^{13}\text{C}$  values are close to solar (Fig. 4). This is within the range measured before on organic “hotspots” in other CR and CM chondrites (e.g., Busemann et al. 2006) and testifies to the pristine nature of analyzed grains. However, one important observation here is that multiglobular organic aggregates in Renazzo sometimes exhibit heterogeneous isotopic compositions, where layers with isotopically highly anomalous nitrogen ( $\delta^{15}\text{N} \sim 700\text{--}2000\%$ ) alternate with areas showing only moderate  $\delta^{15}\text{N}$  values of  $50\text{--}300\%$  (Fig. 3: OM211, Fig. 5: OM210; Table 1; Table S1 in supporting information). All of the

layered aggregates are more strongly depleted in  $^{13}\text{C}$  than the “irregular” aggregates investigated here and the CR bulk insoluble OM (Fig. 4).

### Nanoscale Morphologies of Extracted Organic Particles

BF and HAADF overview images of the FIB lamellae demonstrate that the complex appearance of organic aggregates persists on a nanometer scale (Figs. 6–8). All of the grains are characterized by very low crystallinity, verified by high-resolution imaging of the amorphous organic grains in several regions. It cannot be excluded that tiny sheets of graphene are present in some areas of the grains, but the number and variety of regions observed by STEM-HAADF provides good confidence that the majority of OM in the analyzed grains is amorphous and lacks long-range order. This is also confirmed by the EELS analyses described below, because the presence of graphite-like material would lead to very characteristic fine structure of the C-K absorption edge, including sharp  $\pi^*$  and  $\sigma^*$  peaks at 285 and 291.7 eV, respectively, which are not observed in any of the acquired spectra.

The “OM4” hotspot characterized above by SEM imaging presents a fine-grained mixture of aggregated OM with silicates (Fig. 2). In the TEM, this organic aggregate appears as small (50–200 nm) oval globules embedded in a homogeneous amorphous silicate groundmass (Fig. 7). In one area, we could document the close association of the organic globules with sheet silicates ( $d$ -spacings of about 0.7 nm in HR images) that are directly attached to the organic grains and seem to bend around and encapsulate them (Fig. 7). Unfortunately, we could not measure the chemical composition of the embedding silicates by conventional TEM energy-dispersive X-ray spectroscopy (EDX), because the FIB lamella was lost during transport. If the organic globules are associated with amorphous silicates, the composition of this material could give important clues about nebular and parent body processes (e.g., Hopp and Vollmer 2017). A different texture of OM was documented in grain “B7\_1b” that consists of two relatively large ( $\sim 0.5 \times 1 \mu\text{m}^2$ ) globular oval grains that are clearly separated from the surrounding matrix (Figs. 2 and 7). The same is true for grains “OM164” and “OM166” that consist of huge areas of carbonaceous material with fine lines of minerals dispersed within (Figs. 6 and 8). We note here, however, that the large sizes of extracted organic grains in this work are not necessarily representative of OM in Renazzo as a whole, as the selection of grains large enough for FIB preparation may have introduced an analytical bias into the sample subset. Finally, grain “OM210” is as well relatively large ( $\sim 3 \mu\text{m}$ ), but shows



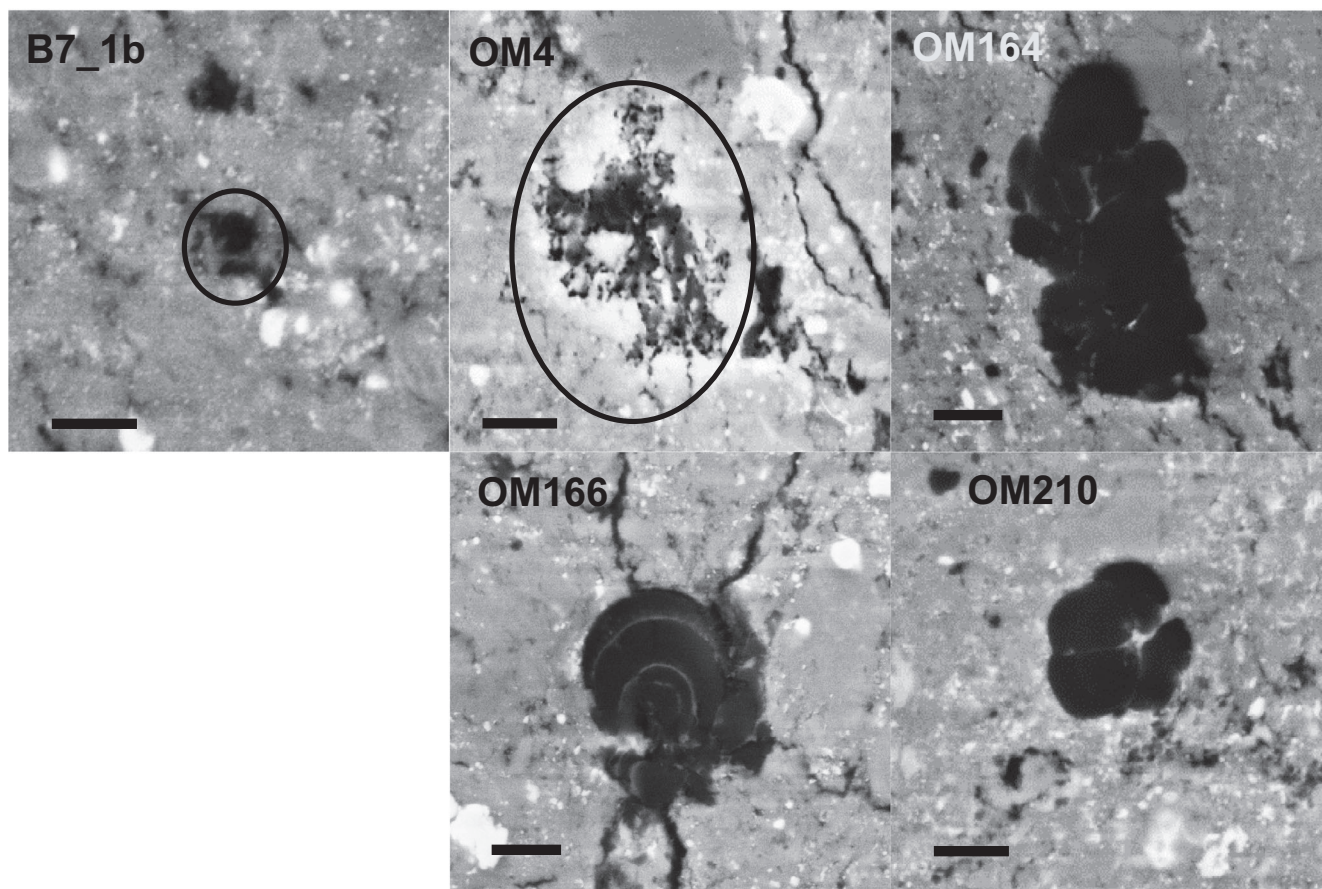


Fig. 2. SEM micrographs of those  $^{15}\text{N}$ -anomalous organic grains that have been FIB-prepared for TEM investigations. B7\_1b) This grain consists of two small globular grains attached to each other. OM4) This hotspot consists of fine-grained OM intermingled with silicates. OM164) This grain represents an aggregate of several smaller, irregular and globular grains. OM166) An example of a distinct “multiglobular” grain with concentric layers of OM separated by brighter fine minerals. OM210) A smaller cluster of several globular particles attached to one another. Scale bar is 2  $\mu\text{m}$  in all images.

an interesting heterogeneous distribution of  $^{15}\text{N}$  enrichment visible in NanoSIMS ion images and also the presence of interspersed fine lines of minerals separating organic areas with different N contents (Figs. 5 and 8).

### Carbon and Nitrogen Functional Chemistry of Extracted Organic Particles

Functional chemistry investigations by EELS provide important information on the local bonding environments of the major elements carbon and nitrogen at the nm-scale. Carbon K-edge functional chemistry consists of the typical onset at around 283.5 eV and a maximum at around 285 eV with varying peak positions due to  $1s-\pi^*$  antibonding transitions from aromatic/olefinic rings. Superimposed fine structure occurs at around 286.5 eV due to aromatic ketone/aldehyde or nitrile bonding, as well as a band at around 288.4–288.7 eV, which can be

assigned to carboxyl bonding environments (Figs. 9–13; all peak positions from Cody et al. 2008). Aliphatic bonding at around 287.3–288.1 eV was also observed in the spectra of the sections studied here, for example, in samples OM4 and OM166 (Fig. 11). Interestingly, in those two grains, it was also not possible to detect any nitrogen. In other work, for example, by Vinogradoff et al. (2017), aliphatic absorption could be only observed as a flank on the strong carboxyl peak in more altered and diffuse portions of the OM. Quantification of the relative abundance of the aromatic fraction relative to the total carbon content as in the work of Vinogradoff et al. (2017) or Changela et al. (2018) was not carried out, because of the inherent uncertainties associated with the quantification of high resolution EEL spectra. It could nevertheless be observed that the relative peak heights of the aromatic 285 eV and the aromatic ketone 286.5 eV fine structure changed on a nm scale across the OM, indicating highly complex O-rich and O-poor functional chemistry on a

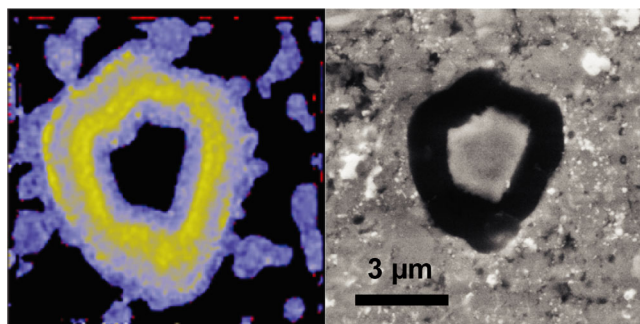


Fig. 3. NanoSIMS–SEM images of the exemplary organic grain OM211 with alternating, heterogeneous  $^{15}\text{N}$  enrichments across the globular grain. Left)  $^{15}\text{N}^{12}\text{C}^-/^{14}\text{N}^{12}\text{C}^-$  ratio NanoSIMS image, with the blue background representing the terrestrial value and the yellow regions showing areas with enhanced  $^{15}\text{N}$  by several hundred per mil. Field of view is  $8\ \mu\text{m}$ . Right) The corresponding SEM image, where the grain has a smooth contrast and encircles a mineral grain, which is not unusual for these types of organics. However, it is also possible that this mineral lies underneath and is seemingly encircled by the organic mantle due to a geometric effect.

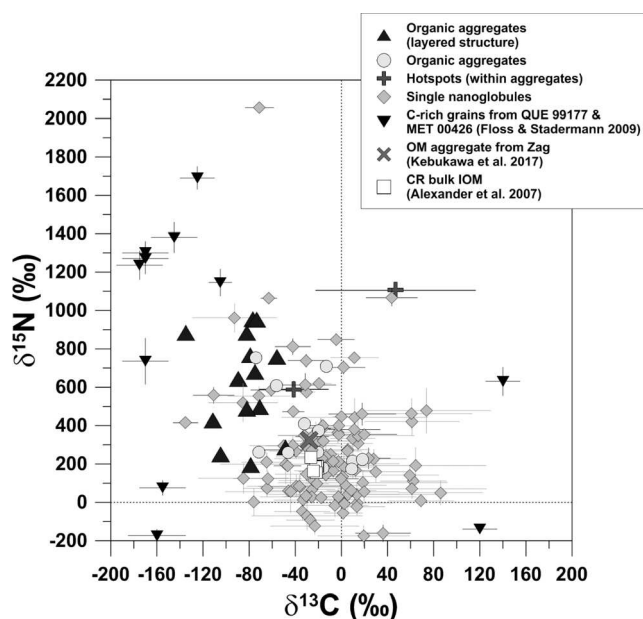


Fig. 4. Carbon and nitrogen isotopic compositions of the Renazzo organic grains in this work obtained by NanoSIMS ion imaging compared to selected literature values. The OM shows only close to solar to depleted  $^{13}\text{C}$  isotopic compositions and  $^{15}\text{N}$  enrichments of up to  $\sim 2000\text{‰}$ , very similar to literature values. Error bars represent one sigma standard deviation from counting statistics only. Data points without error bars represent values with the standard deviation smaller than the symbol.

very small scale within the macromolecular matter. It was possible to reliably quantify elemental N/C and O/C ratios from our broad EEL spectra in the different

grains (Figs. 9–13; Table 2), albeit with relatively large uncertainties by comparison to bulk techniques. Generally, the measured N/C and O/C ratios are around 0.1, which is consistent with what has been observed before.

Within three grains, namely B7\_1b, OM164, and OM210, we could document the N-K edge functionality whose onset lies at around 400 eV (Figs. 9c, 12c, 13c). Although nitrogen was easily detected and measured by NanoSIMS in these organic grains even at trace level, the identification of the N-K edge fine structure in EELS was probably only possible in these specific lamellae due to the higher abundance of N atoms in those OM samples (atomic N/C around 0.1; Table 2). Several spectral bands could be observed with varying intensity, superimposed as fine structure onto the typical prominent combination of  $\pi^*$  and  $\sigma^*$  antibonding transitions, that give clues about the functional makeup of nitrogen within the OM. A 401.4–401.9 eV band can likely be assigned to the amidyl-N ( $\text{NH}_x[\text{C}=\text{O}]\text{C}$  1s- $\pi^*$  transition, given the concurrent high intensity of the ketone functional bands at the C-K edge (Cody et al. 2008). However, this band was only weakly detected in grain OM210 (Fig. 13). In grains B7\_1b and OM210, further fine structure occurs at higher energies, around 403.2 eV, which can be due to 1s-3p/ $\sigma^*$  transitions due to differently bonded C-NH $_x$ -(amine) functional groups (at around 402.2 eV), for example, in aliphatic or aromatic carbon molecules or amide nitrogen ( $\text{CO-NR}_2$ ) at around 402.6 eV. The intensity of the amine transition is proportional to the number of hydrogen atoms attached to the amine group, for example, whether it is a primary ( $\text{NH}_2\text{-R}$ ), secondary ( $\text{R-NH-R}$ ), or tertiary ( $\text{N-R}_3$ ) amine group (Cody et al. 2008). In several spectra, we observe strong absorption at around 403 eV (Figs. 9c and 13c), which can be assigned to this functional group or alternatively to amide nitrogen. A definite assignment is difficult to establish given the relatively low signal-to-noise ratio of the data resulting from the constraints of keeping the electron dose low to avoid potential beam damage with our energy resolution. However, because amine functional chemistry has been detected by bulk techniques in other work as well (e.g., Cody and Alexander 2017), we more likely assume that N-H amine functional groups are present, which are slightly affected by some H loss and transformation to amide nitrogen. We therefore likely observe a mixture of both amine and amide nitrogen at around 403 eV. Nitrogen heterocycles with one or two N atoms within aromatic rings (pyrrole,  $\text{C}_4\text{H}_4\text{NH}$ , or imidazole,  $\text{C}_3\text{H}_4\text{N}_2$ ) also exhibit absorption energies within the range 402–403 eV, so it is difficult to disentangle this band from the pure amine or amide functional groups without heteroatoms. However, N-



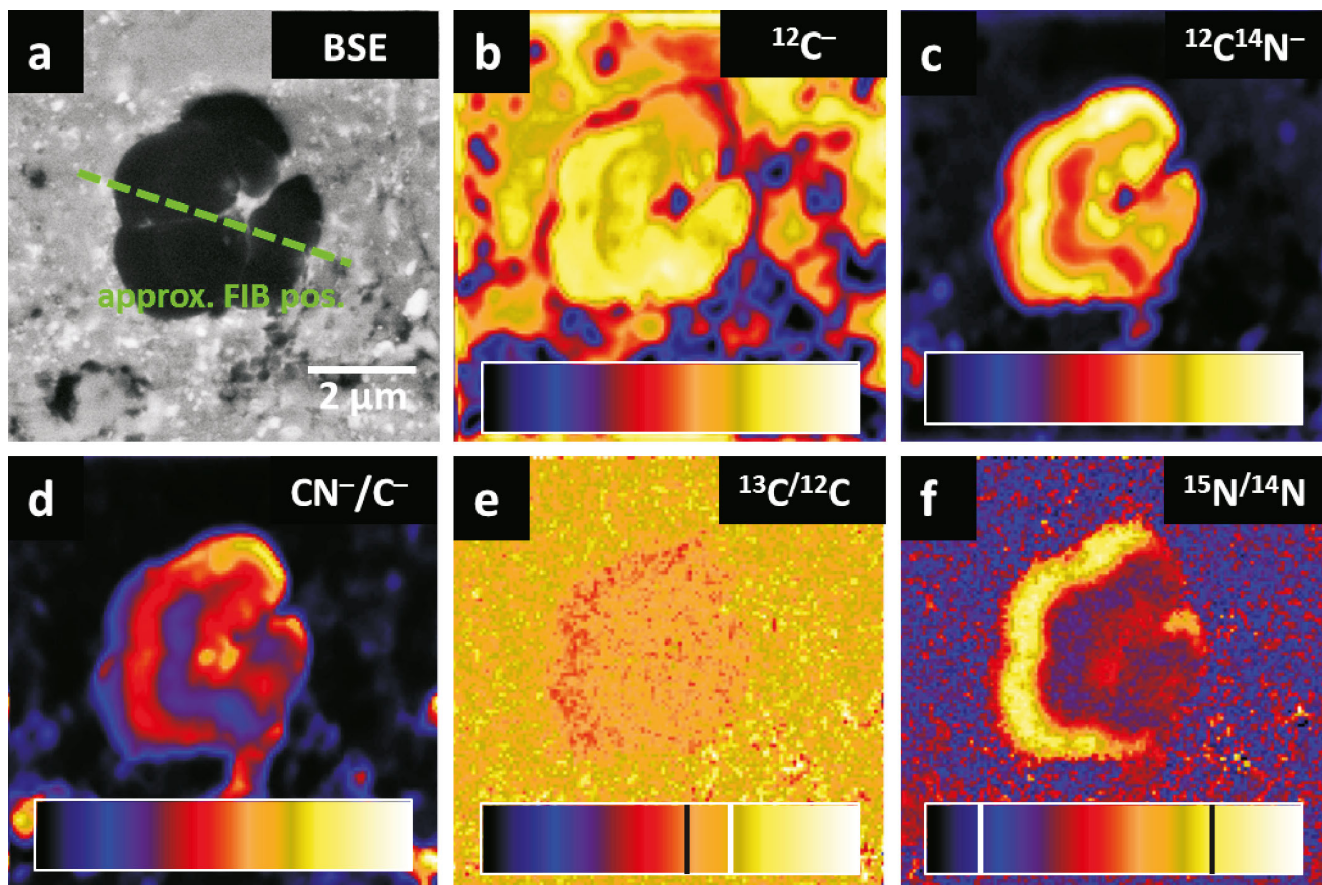


Fig. 5. a) SEM micrograph with the location of the FIB lamella. b and c) NanoSIMS secondary ion images of  $^{12}\text{C}^-$  and  $^{12}\text{C}^{14}\text{N}^-$ , where the distribution of carbon and nitrogen is clearly visible. d–f) Ion ratio images of C/N, carbon, and nitrogen isotopic compositions of the grain. The heterogeneous distribution of alternating nitrogen contents across the grain can be seen in panel (d). The heterogeneous  $^{15}\text{N}$  enrichment across the globular grain is obvious from panel (f). White lines within the color scale bars refer to the solar values in the isotope ratio images. For the  $^{13}\text{C}/^{12}\text{C}$  isotopic ratio map, this corresponds to a value of  $0.011237$  ( $\delta^{13}\text{C}_{\text{PDB}} = -29\text{‰}$ ), and for the  $^{15}\text{N}/^{14}\text{N}$  isotopic ratio map to a value of  $3.676 \times 10^{-3}$  ( $\delta^{15}\text{N}_{\text{air}} = 0$ ). The black lines correspond to a minimum value of about  $-170\text{‰}$  for the  $^{13}\text{C}/^{12}\text{C}$  ratio map, and to a maximum value of about  $+1670\text{‰}$  for the  $^{15}\text{N}/^{14}\text{N}$  ratio map. Field of view is  $8 \mu\text{m}$ .

heterocycles like imidazole and pyrrole also show additional absorption at around  $406.9 \text{ eV}$  (Leinweber et al. 2007), which is not present in our N-K edge spectra. Nitrogen heterocycles are potentially very interesting molecules relevant for the emergence of life, because they represent the building blocks of nucleobases (Martins 2011). Further fine structure at the N-K edge at around  $403.5 \text{ eV}$  could be ascribed to the presence of urea nitrogen ( $\text{CO}[\text{NH}_2]_2$ ), which is another plausible candidate given our prominent C-O bonding functionality at the C-K edge. However, nitrogen in the form of nitro groups ( $-\text{NO}_2$ ), which could be a secondary oxygenation product of amines, also absorbs in that energy range (Cody and Alexander 2017) and could be present as well. We also occasionally observed weak energy absorption at around  $405 \text{ eV}$  in grains B7\_1b (Fig. 9c), OM164 (Fig. 12c), and OM210 (Fig. 13c). This band cannot be assigned to the

functional groups described above, but could be due to the presence of even more oxygenated N-bearing functional groups such as nitrate (Alexander et al. 2017), which supports the observation that these N-containing functional groups are highly prone to alteration reactions.

To summarize our observations on N-K edge functionality, we could find strong indications of organic N-bearing molecules with amine or amide functional chemistry, as well as possible N-heterocycles at around  $403 \text{ eV}$ . Furthermore, either urea nitrogen or nitro groups due to oxygenation reactions could account for strong energy absorption at around  $403.5 \text{ eV}$ . The relative intensities of the different bands vary on a nanometer scale in all spectrum images, an observation that is only made possible by the probe size of the STEM-EELS technique deployed here. It is therefore well conceivable that nitrogen functional

Table 1. List of all grains and regions within selected grains (in *italics*) with heterogeneous compositions detected by NanoSIMS. The N-, and C-isotopic compositions are given as  $\delta$ -values (deviation from terrestrial standard in per mil), together with the respective  $^{12}\text{C}^{14}\text{N}^-/^{12}\text{C}^-$  ratios. For  $\delta^{15}\text{N}$ -values, we estimate an additional uncertainty of  $\sim 15\%$  due to unknown matrix effects for the organic material. Reported errors in the table are therefore only due to counting statistics and refer to  $1\sigma$ .

Grain	$\delta^{15}\text{N}$ (‰)	$\delta^{13}\text{C}$ (‰)	$^{12}\text{C}^{14}\text{N}^-/^{12}\text{C}^-$	Type
REN_OM_002	710 ± 10	-10 ± 10	9.2	Agg. (gl.)
REN_OM_002B	350 ± 20	20 ± 30	5.9	nanoglobule
REN_OM_004	410 ± 10	-30 ± 10	4.0	Agg. (irr.)
REN_OM_006	210 ± 10	10 ± 10	1.5	Agg. (irr.)
REN_OM_007	260 ± 10	-20 ± 10	2.4	Agg. (irr.)
REN_OM_039	610 ± 10	-60 ± 10	1.2	Agg. (gl.)
REN_OM_039B	380 ± 20	-20 ± 10	0.7	Nanoglobule
REN_OM_045	500 ± 10	-70 ± 10	0.2	Agg. (gl.)
<i>Intermed. high-<sup>15</sup>N-shell</i>	970 ± 40	-80 ± 10	0.2	
<i>Inner high-<sup>15</sup>N-shell</i>	1150 ± 40	-100 ± 10	0.1	
<i>Top high-<sup>15</sup>N-area</i>	780 ± 40	-80 ± 10	0.2	
<i>Outer low-<sup>15</sup>N-shell</i>	160 ± 20	-40 ± 10	0.4	
<i>Inner part</i>	560 ± 20	-70 ± 10	0.2	
REN_OM_045B	120 ± 70	0 ± 20	0.2	Nanoglobule
REN_OM_045C	230 ± 60	20 ± 20	0.4	Nanoglobule
REN_OM_069	430 ± 10	-110 ± 10	0.6	Agg. (gl.)
REN_OM_069C	560 ± 30	-110 ± 20	0.7	Nanoglobule
REN_OM_069D	610 ± 60	-30 ± 30	0.8	Nanoglobule
REN_OM_069E	590 ± 40	-60 ± 20	1.3	Nanoglobule
REN_OM_069F	740 ± 30	-30 ± 20	1.3	Nanoglobule
REN_OM_069G	850 ± 30	-10 ± 20	1.3	Nanoglobule
REN_OM_069H	270 ± 40	-50 ± 20	0.9	Nanoglobule
REN_OM_069I	-160 ± 40	40 ± 20	0.6	Nanoglobule
REN_OM_069J	390 ± 50	-20 ± 20	0.3	Nanoglobule
REN_OM_070A	950 ± 10	-70 ± 10	1.9	Agg. (irr.)
REN_OM_070B	880 ± 10	-80 ± 10	1.1	Agg. (irr.)
REN_OM_097	290 ± 10	-50 ± 10	0.8	Agg. (gl.)
REN_OM_097B	700 ± 40	0 ± 20	1.2	nanoglobule
REN_OM_164	770 ± 10	-80 ± 10	2.7	Agg. (gl.)
<i>Area 1</i>	850 ± 10	-80 ± 10	3.8	
<i>Area 2</i>	810 ± 20	-70 ± 10	2.5	
<i>Area 3</i>	720 ± 10	-80 ± 10	2.4	
<i>Area 4</i>	1200 ± 20	-90 ± 20	4.2	
<i>Area 5</i>	1140 ± 10	-80 ± 10	2.7	
<i>Area 6</i>	1000 ± 10	-80 ± 10	2.9	
<i>Area 7</i>	810 ± 10	-110 ± 10	3.4	
<i>Hotspot (Area 8)</i>	1040 ± 10	-90 ± 10	3.2	
<i>Area 9</i>	1010 ± 20	-100 ± 10	4.4	
<i>Area 10</i>	940 ± 20	-70 ± 10	3.3	
<i>Area 11</i>	430 ± 10	-80 ± 10	2.3	
<i>Area 12</i>	470 ± 20	-70 ± 10	2.3	
<i>Area 13</i>	530 ± 10	-80 ± 10	2.0	
<i>Area 14</i>	690 ± 20	-60 ± 10	2.0	
<i>Area 15</i>	600 ± 10	-90 ± 10	2.5	
<i>Area 16</i>	590 ± 30	-60 ± 30	3.0	
REN_OM_165A	490 ± 10	-80 ± 10	1.0	Agg. (gl.)
REN_OM_165B	30 ± 10	-40 ± 10	0.9	Agg. (gl.)
REN_OM_165C	2060 ± 20	-70 ± 10	2.1	nanoglobule
REN_OM_166	200 ± 10	-80 ± 10	0.2	Agg. (gl.)
<i>Area 1</i>	720 ± 40	-110 ± 10	0.2	

Table 1. *Continued.* List of all grains and regions within selected grains (in *italics*) with heterogeneous compositions detected by NanoSIMS. The N-, and C-isotopic compositions are given as  $\delta$ -values (deviation from terrestrial standard in per mil), together with the respective  $^{12}\text{C}^{14}\text{N}^-/^{12}\text{C}^-$  ratios. For  $\delta^{15}\text{N}$ -values, we estimate an additional uncertainty of  $\sim 15\%$  due to unknown matrix effects for the organic material. Reported errors in the table are therefore only due to counting statistics and refer to  $1\sigma$ .

Grain	$\delta^{15}\text{N}$ (‰)	$\delta^{13}\text{C}$ (‰)	$^{12}\text{C}^{14}\text{N}^-/^{12}\text{C}^-$	Type
<i>Area 2</i>	130 ± 20	-70 ± 10	0.1	
<i>Area 3</i>	80 ± 40	-100 ± 10	0.1	
<i>Area 4</i>	260 ± 50	-80 ± 10	0.2	
REN_OM_190	640 ± 10	-90 ± 10	1.4	Agg. (gl.)
REN_OM_194	960 ± 10	-80 ± 10	1.1	Agg. (gl.)
REN_OM_206	250 ± 10	-110 ± 10	2.1	Agg. (gl.)
REN_OM_206B	420 ± 20	-140 ± 10	2.0	Nanoglobule
REN_OM_206C	30 ± 10	-30 ± 10	2.5	Vein
REN_OM_206D	460 ± 60	20 ± 30	1.0	Nanoglobule
REN_OM_206E	1070 ± 50	40 ± 20	1.6	Nanoglobule
REN_OM_207_1A	220 ± 10	20 ± 10	0.7	Agg. (irr.)
REN_OM_207_1B	40 ± 10	-40 ± 10	1.5	Vein
REN_OM_207_1C	180 ± 10	-20 ± 10	1.2	Agg. (irr.)
REN_OM_207_1D	210 ± 10	-10 ± 10	0.9	Agg. (irr.)
REN_OM_207_2A	170 ± 10	10 ± 10	0.3	Agg. (irr.)
REN_OM_207_2B	20 ± 10	10 ± 10	1.0	Vein
REN_OM_208	750 ± 10	-70 ± 10	0.5	Agg. (irr.)
REN_OM_208B	260 ± 10	-50 ± 10	0.5	Agg. (irr.)
REN_OM_209	260 ± 10	-70 ± 10	1.2	Agg. (gl.)
REN_OM_210	880 ± 10	-140 ± 10	1.4	Agg. (gl.)
<i>Outer high <sup>15</sup>N-shell</i>	1670 ± 10	-170 ± 10	1.7	
<i>Inner high <sup>15</sup>N-shell</i>	530 ± 10	-140 ± 10	1.7	
<i>Outer low <sup>15</sup>N-shell</i>	230 ± 10	-120 ± 10	1.1	
<i>Inner low <sup>15</sup>N-part</i>	300 ± 10	-120 ± 10	1.3	
REN_OM_211	680 ± 10	-80 ± 10	2.5	Agg. (gl.)
REN_OM_211B	400 ± 30	-20 ± 10	0.7	Nanoglobule
REN_OM_213	760 ± 10	-60 ± 10	1.0	Agg. (gl.)
REN_OM_213B	890 ± 90	-60 ± 10	1.0	Nanoglobule
REN_OM_214	370 ± 10	-20 ± 10	0.7	Agg. (irr.)
REN_OM_214B	470 ± 30	-40 ± 10	0.5	Nanoglobule
REN_OM_214C	810 ± 40	-40 ± 20	0.7	Nanoglobule
REN_OM_214D	380 ± 40	10 ± 20	0.8	Nanoglobule
REN_OM_214E	270 ± 40	-30 ± 10	0.4	Nanoglobule
REN_OM_214F	190 ± 30	-50 ± 10	0.7	Nanoglobule
REN_OM_214G	340 ± 40	-30 ± 10	0.8	Nanoglobule
REN_B_1_1	750 ± 30	10 ± 20	2.0	Nanoglobule
REN_B_1_2	420 ± 70	60 ± 40	1.7	Nanoglobule
REN_B_1_3	110 ± 40	60 ± 30	1.2	Nanoglobule
REN_B_1_4	70 ± 50	-70 ± 20	0.7	Nanoglobule
REN_B_1_5	80 ± 80	-40 ± 40	0.8	Nanoglobule
REN_B_1_6	200 ± 100	-50 ± 60	1.5	Nanoglobule
REN_B_2_1	280 ± 40	10 ± 20	1.4	Nanoglobule
REN_B_2_2	160 ± 60	30 ± 30	1.2	Nanoglobule
REN_B_2_3	-50 ± 50	-30 ± 20	0.9	Nanoglobule
REN_B_2_4	440 ± 100	10 ± 60	2.2	Nanoglobule
REN_B_2_5	160 ± 40	-20 ± 20	1.0	Nanoglobule
REN_B_2_6	70 ± 30	-30 ± 20	1.1	Nanoglobule
REN_B_2_7	-206 ± 50	20 ± 40	1.4	Nanoglobule
REN_B_2_8	-70 ± 70	-30 ± 50	1.3	Nanoglobule



Table 1. *Continued.* List of all grains and regions within selected grains (in *italics*) with heterogeneous compositions detected by NanoSIMS. The N-, and C-isotopic compositions are given as  $\delta$ -values (deviation from terrestrial standard in per mil), together with the respective  $^{12}\text{C}^{14}\text{N}^-/^{12}\text{C}^-$  ratios. For  $\delta^{15}\text{N}$ -values, we estimate an additional uncertainty of  $\sim 15\text{‰}$  due to unknown matrix effects for the organic material. Reported errors in the table are therefore only due to counting statistics and refer to  $1\sigma$ .

Grain	$\delta^{15}\text{N}$ (‰)	$\delta^{13}\text{C}$ (‰)	$^{12}\text{C}^{14}\text{N}^-/^{12}\text{C}^-$	Type
REN_B_2_9	100 ± 70	20 ± 70	6.7	Nanoglobule
REN_B_2_10	0 ± 40	10 ± 30	2.2	Nanoglobule
REN_B_2_11	-60 ± 30	0 ± 20	1.2	Nanoglobule
REN_B1_1	250 ± 20	-10 ± 10	1.1	Nanoglobule
REN_B1_2	310 ± 30	20 ± 10	1.2	Nanoglobule
REN_B1_3	250 ± 30	-20 ± 20	1.9	Nanoglobule
REN_B1_4	60 ± 30	-50 ± 20	1.5	Nanoglobule
REN_B1_5	30 ± 40	-30 ± 30	1.7	Nanoglobule
REN_B1_6	10 ± 20	0 ± 20	3.8	Nanoglobule
REN_B1_7	170 ± 40	10 ± 20	1.2	Nanoglobule
REN_B2_1	190 ± 30	-10 ± 10	1.0	Nanoglobule
REN_B2_2	-90 ± 30	-30 ± 20	1.1	Nanoglobule
REN_B2_3	150 ± 40	-30 ± 30	1.7	Nanoglobule
REN_B2_4	-120 ± 40	-20 ± 40	2.2	Nanoglobule
REN_B2_5	10 ± 30	-30 ± 30	1.5	Nanoglobule
REN_B2_6	180 ± 60	0 ± 30	0.7	Nanoglobule
REN_B3_1	-20 ± 50	10 ± 20	0.8	Nanoglobule
REN_B3_2	10 ± 30	70 ± 30	2.2	Nanoglobule
REN_B3_3	120 ± 80	-90 ± 40	1.1	Nanoglobule
REN_B3_4	70 ± 50	60 ± 70	4.8	Nanoglobule
REN_B3_5	40 ± 60	10 ± 80	5.7	Nanoglobule
REN_B3_6	-20 ± 60	-10 ± 30	0.8	Nanoglobule
REN_B3_7	290 ± 70	-30 ± 40	1.0	Nanoglobule
REN_B3_8	60 ± 60	20 ± 30	1.2	Nanoglobule
REN_B3_9	0 ± 70	-80 ± 40	1.2	Nanoglobule
REN_B3_10	200 ± 80	10 ± 40	1.1	Nanoglobule
REN_B3_11	350 ± 50	-30 ± 20	1.1	Nanoglobule
REN_B3_12	50 ± 60	90 ± 40	1.1	Nanoglobule
REN_B3_13	210 ± 50	-70 ± 20	1.0	Nanoglobule
REN_B4_1	960 ± 80	-90 ± 40	1.3	Nanoglobule
REN_B4_2	330 ± 60	10 ± 20	0.6	Nanoglobule
REN_B4_3	350 ± 70	-20 ± 30	1.1	Nanoglobule
REN_B4_4	310 ± 70	-20 ± 20	0.6	Nanoglobule
REN_B4_5	110 ± 60	-20 ± 30	0.9	Nanoglobule
REN_B4_6	320 ± 70	-20 ± 30	0.9	Nanoglobule
REN_B4_7	350 ± 80	10 ± 50	1.3	Nanoglobule
REN_B5_1	520 ± 100	-90 ± 30	0.5	Nanoglobule
REN_B5_2	240 ± 60	-10 ± 40	1.5	Nanoglobule
REN_B5_3	190 ± 100	60 ± 60	1.5	Nanoglobule
REN_B5_4	80 ± 60	-40 ± 40	1.3	Nanoglobule
REN_B5_5	210 ± 20	-10 ± 10	0.4	Nanoglobule
REN_B5_6	160 ± 50	-10 ± 30	1.9	Nanoglobule
REN_B5_7	480 ± 120	70 ± 60	1.2	Nanoglobule
REN_B5_8	-10 ± 20	0 ± 10	1.3	Nanoglobule
REN_B5_9	90 ± 110	0 ± 40	0.4	Nanoglobule
REN_B5_10	60 ± 110	-40 ± 60	0.7	Nanoglobule
REN_B5_11	40 ± 80	10 ± 50	1.0	Nanoglobule
REN_B6_1	280 ± 10	0 ± 10	1.5	Nanoglobule
REN_B6_2	300 ± 20	-50 ± 10	1.6	Nanoglobule

Table 1. *Continued.* List of all grains and regions within selected grains (in *italics*) with heterogeneous compositions detected by NanoSIMS. The N-, and C-isotopic compositions are given as  $\delta$ -values (deviation from terrestrial standard in per mil), together with the respective  $^{12}\text{C}^{14}\text{N}^-/^{12}\text{C}^-$  ratios. For  $\delta^{15}\text{N}$ -values, we estimate an additional uncertainty of  $\sim 15\%$  due to unknown matrix effects for the organic material. Reported errors in the table are therefore only due to counting statistics and refer to  $1\sigma$ .

Grain	$\delta^{15}\text{N}$ (‰)	$\delta^{13}\text{C}$ (‰)	$^{12}\text{C}^{14}\text{N}^-/^{12}\text{C}^-$	Type
REN_B6_3	210 ± 40	0 ± 20	1.0	Nanoglobule
REN_B6_4	270 ± 40	-40 ± 20	1.3	Nanoglobule
REN_B6_5	30 ± 40	0 ± 70	1.1	Nanoglobule
REN_B6_6	130 ± 40	0 ± 30	1.5	Nanoglobule
REN_B6_7	60 ± 40	10 ± 20	1.5	Nanoglobule
REN_B6_8	230 ± 20	-30 ± 10	1.4	Nanoglobule
REN_B6_9	100 ± 20	-20 ± 10	1.1	Nanoglobule
REN_B6_10	290 ± 30	-30 ± 20	1.4	Nanoglobule
REN_B6_11	300 ± 50	-40 ± 40	1.4	Nanoglobule
REN_B6_12	140 ± 60	60 ± 30	0.7	Nanoglobule
REN_B6_13	370 ± 60	0 ± 30	1.2	Nanoglobule
REN_B6_14	230 ± 50	30 ± 30	1.4	Nanoglobule
REN_B6_15	30 ± 30	-30 ± 20	1.0	Nanoglobule
REN_B6_16	350 ± 30	0 ± 20	1.2	Nanoglobule
REN_B6_17	550 ± 50	-0 ± 30	1.0	Nanoglobule
REN_B6_18	230 ± 60	-20 ± 40	1.4	Nanoglobule
REN_B6_19	80 ± 60	-40 ± 40	1.6	Nanoglobule
REN_B6_20	460 ± 80	60 ± 50	2.1	Nanoglobule
REN_B7_1a	620 ± 20	-20 ± 10	2.3	Agg. (irr.)
REN_B7_1b	580 ± 20	-30 ± 10	1.2	Agg. (irr.)
REN_B7_2	450 ± 10	0 ± 10	1.9	Agg. (irr.)
REN_B7_3	140 ± 30	-10 ± 20	1.6	Nanoglobule
REN_B7_4	270 ± 20	10 ± 10	1.1	Nanoglobule
REN_B7_5	400 ± 20	0 ± 10	1.0	Nanoglobule
REN_B7_6	120 ± 40	-60 ± 30	1.2	Nanoglobule

“Agg.” = Aggregate, “irr.” = irregular, “gl.” = globular.

chemistry is as complex as the carbon bonding environments, and further complementary synchrotron work is clearly necessary to draw tighter conclusions about the functional makeup of nitrogen within this energy range, albeit with a poorer spatial sensitivity.

### Low Loss Spectroscopy of Extracted Organic Grains

Recent achievements in the design of electron gun monochromators have allowed the detection of absorption bands by EELS techniques with an unprecedented energy resolution below 0.01 eV (Krivanek et al. 2014). This “meV” energy loss regime has opened up new avenues of research in material sciences. The improved energy resolution facilitates for instance the detection of hydrogen or helium K absorption edges at very low energy losses of around 5–25 eV (Bradley et al. 2014; Blackmur et al. 2018). Importantly, by reducing the electron energy spread to only about 0.01 eV, it is also now possible to detect very weak bands on the tail of the zero loss peak below 0.2 eV,

including peaks associated with the optical response of materials in the deep infrared or THz regime, as well as vibrational peaks traditionally only detected with Raman or infrared spectroscopy (e.g., Hage et al. 2018). Although the energy resolution of these ultra-high-resolution monochromated electron microscopes is for now inferior to that of conventional Raman or IR spectrometer gratings, where the typical wave number resolution is on the order of  $1\text{ cm}^{-1}$  ( $=0.12\text{ meV}$ , to convert from  $\text{cm}^{-1}$  to eV, divide by 8066, Krivanek et al. 2014), as discussed in the following section, the superior spatial sensitivity of vibrational spectroscopy in the electron microscope is a clear advantage compared to optical spectroscopy techniques. Furthermore, recent instrumentation developments promise to improve the achievable resolution to better than 5 meV ( $\sim 40\text{ cm}^{-1}$ ), which in the future should allow for a more direct comparison with Raman or IR data (Hachtel et al. 2019).

We also note that differences in selection rules among EELS, Raman, and Fourier transform-IR (FT-IR) result in differences in activated modes and, hence,

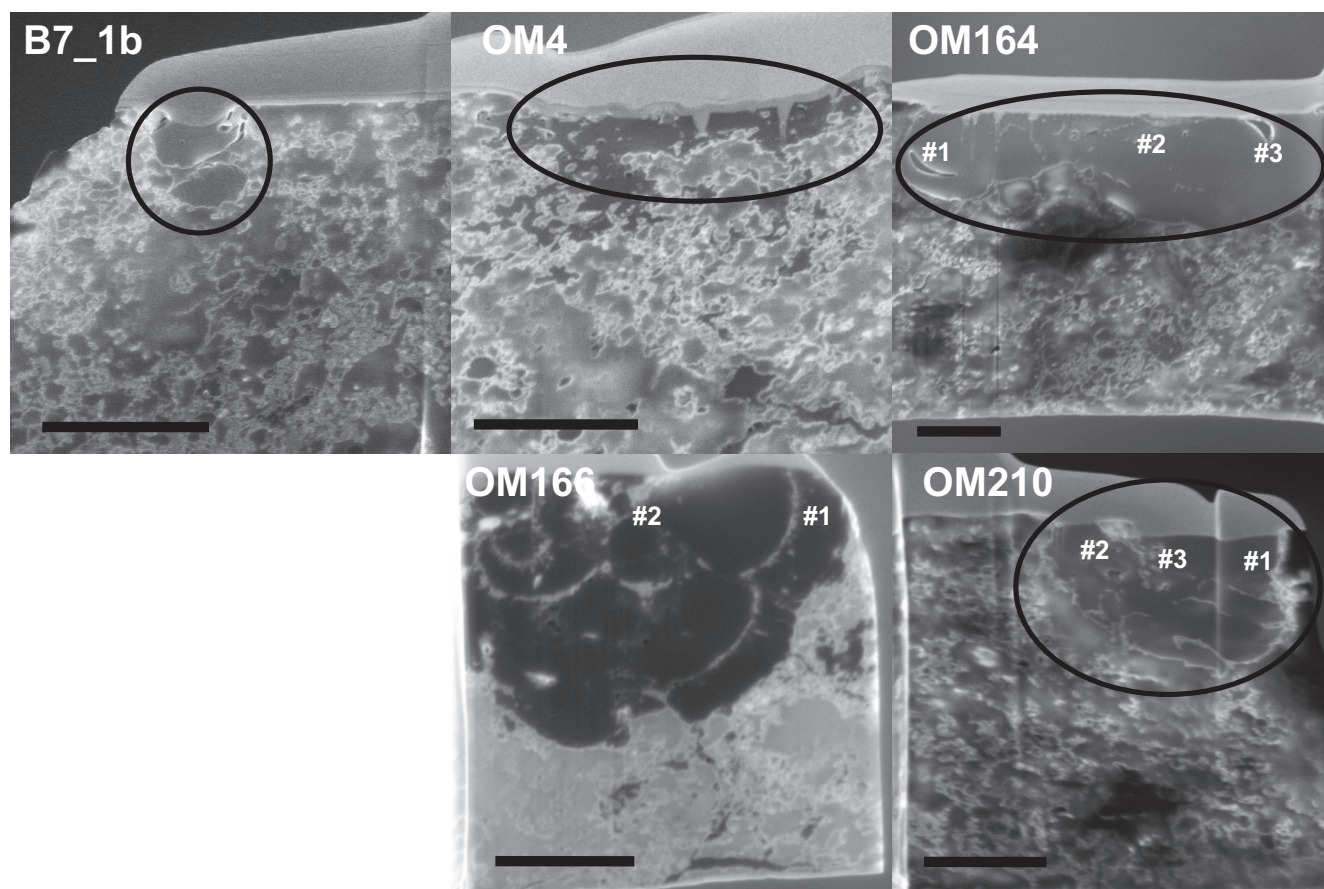


Fig. 6. FIB-SEM images of the five extracted OM lamellae with the regions of interest encircled. The regions within OM164, OM166, and OM210 with acquired EEL spectra and close-up images in subsequent figures are indicated by numbers. Scale bar is 2  $\mu\text{m}$  in every panel.

peak positions, as well as relative intensities. A direct comparison to optical data, while instructive, can therefore be challenging (e.g., Hachtel et al. 2019). However, the electron microscopy community's understanding of the processes underlying vibrational EELS in the STEM is progressing very rapidly. Theoretical tools to model these interactions *ab initio* are now available and excellent quantitative agreement in both peak positions and intensities has now been demonstrated in a number of systems (Hachtel et al. 2019; Nicholls et al. 2019; Senga et al. 2019).

Organic matter in meteorites has long been characterized by Raman spectroscopy techniques on a  $\mu\text{m}$  scale (e.g., Bonal et al. 2007; Busemann et al. 2010; Quirico et al. 2014). The two major features present in the Raman spectra of amorphous carbonaceous matter are the so-called “D” (“defects”) and “G” (“graphite”) bands between 1000 and 1600  $\text{cm}^{-1}$ . These bands are characteristic of polyaromatic OM and can be used to determine the peak temperatures of thermally altered OM in petrologic type  $>3$  chondrites, because the lateral

size of polyaromatic domains and the general structural order has an effect on the positions and spectral widths of these two bands (see discussion in Bonal et al. 2007). In this work, we have used a monochromated electron beam ( $\Delta E = 0.018$  eV, thus corresponding to an energy resolution of  $\sim 145$   $\text{cm}^{-1}$ ) to characterize the Renazzo OM by spatially resolved vibrational spectroscopy in the STEM, in direct correlation to core-loss EELS spectroscopy acquired in immediately adjacent areas. To our knowledge, this is the first time that such an experiment has been performed on a meteoritic OM. Due to the limitations discussed above, we have refrained from a detailed quantitative analysis of the spectral signature, and we stress that we merely provide a qualitative interpretation of peak positions based on similar bands observed in optical spectra of polyaromatic OM.

In grain B7-1b, we could identify several characteristic energy loss bands with varying intensity across the grain at around 0.17 and 0.2 eV on the tail of the zero loss peak (Fig. 10). These two bands correspond



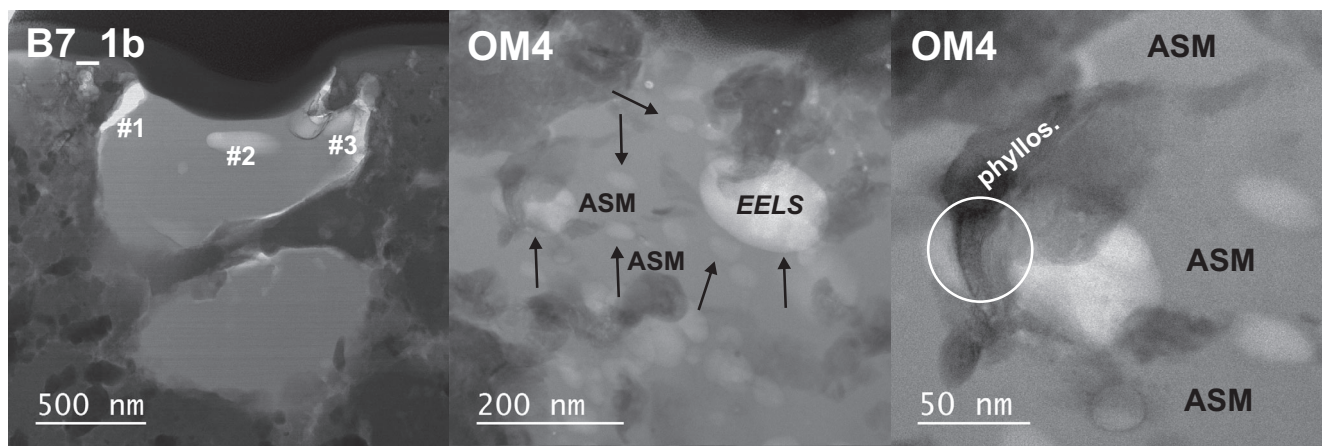


Fig. 7. STEM-BF overview images of selected regions within the extracted grains of interest. Grain B7\_1b consists of two globular amorphous and homogeneous grains well separated from the surrounding Fe-rich matrix. The three thin enough regions from which EEL spectra were acquired are indicated as well (#1–3). Grain OM4 consists of several very small oval organic globules (some of them arrow marked) embedded in an amorphous silicate material (“ASM,” middle panel). The globule from which EEL spectra were acquired (Fig. 11) is marked. In one occasion, the globule is clearly attached to phyllosilicates (“phyllos.”) with a  $d$ -spacing of about 0.7 nm encapsulating the organic globule (right panel, encircled).

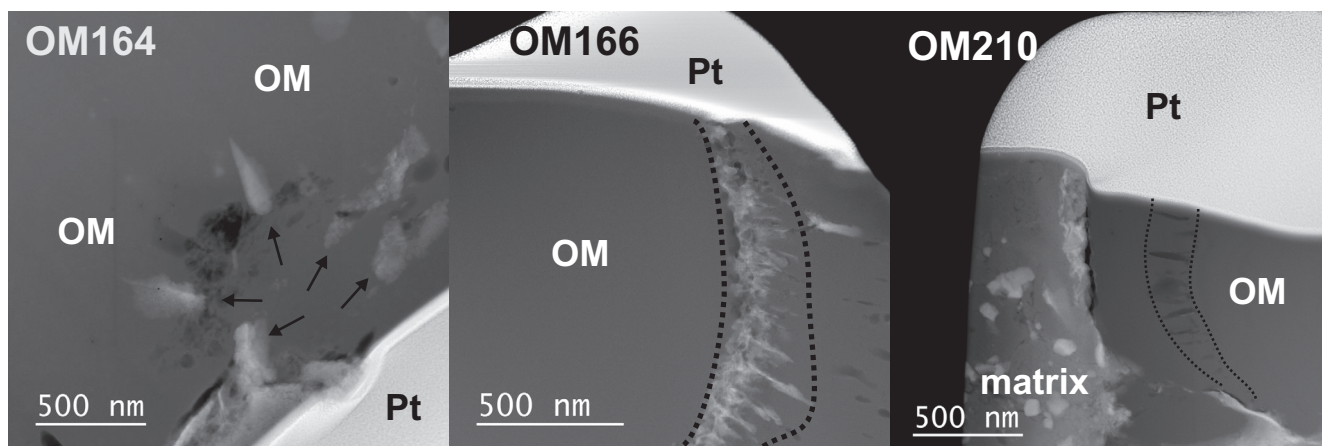


Fig. 8. STEM-HAADF overview images of selected regions within the extracted grains of interest. In OM164 (region #2 in Fig. 6) and OM166 (region #1 in Fig. 6), the organic matter is crosscut by lath-shaped silicates in a circular manner (marked by arrows and a dotted line, respectively). In grain OM210 (region #1 in Fig. 6), these lines from the layered texture of the grain can be observed as well (dotted lines). The Pt cap and regions of organic matter (OM) and matrix are indicated in each panel.

to about  $1360$  and  $1630\text{ cm}^{-1}$ , and match favorably to the D- and G-bands known from Raman spectroscopy, within the resolution limitations of our instrument. Reported literature values for the G-band are typically lower than our measurement (between  $1578$  and  $1599\text{ cm}^{-1}$  in Busemann et al. [2010], for instance), so that an alternative assignment could be made to the D' band, reported at  $1620\text{ cm}^{-1}$ , which arises from defects in the aromatic structure. Complementary assignments from FT-IR spectroscopy acquired on IOM from meteorites (Kebukawa et al. 2011) suggest that the C=C stretch mode at around  $1580\text{--}1600\text{ cm}^{-1}$  as well as the C-O stretch mode at around  $1100\text{ cm}^{-1}$  may also contribute to

the vibrational intensity we observe in our EELS data. Symmetric or asymmetric bending modes of aliphatic  $\text{CH}_3$  at  $1375$  and  $1455\text{ cm}^{-1}$ , respectively, could also account for some of these features. In complex organic systems, a superposition of peaks is likely (e.g., Ferralis et al. 2016), and all these spectral signatures may well be present in our data. However, from our core loss analysis, and without any strong indication of aliphatic bonding within EEL spectra, the G-band would seem a more likely dominant contribution to observed spectra.

In particular, we note tentatively that the relative peak heights of the  $0.17$  and  $0.2\text{ eV}$  feature are around 1, which would be very similar to what is observed in

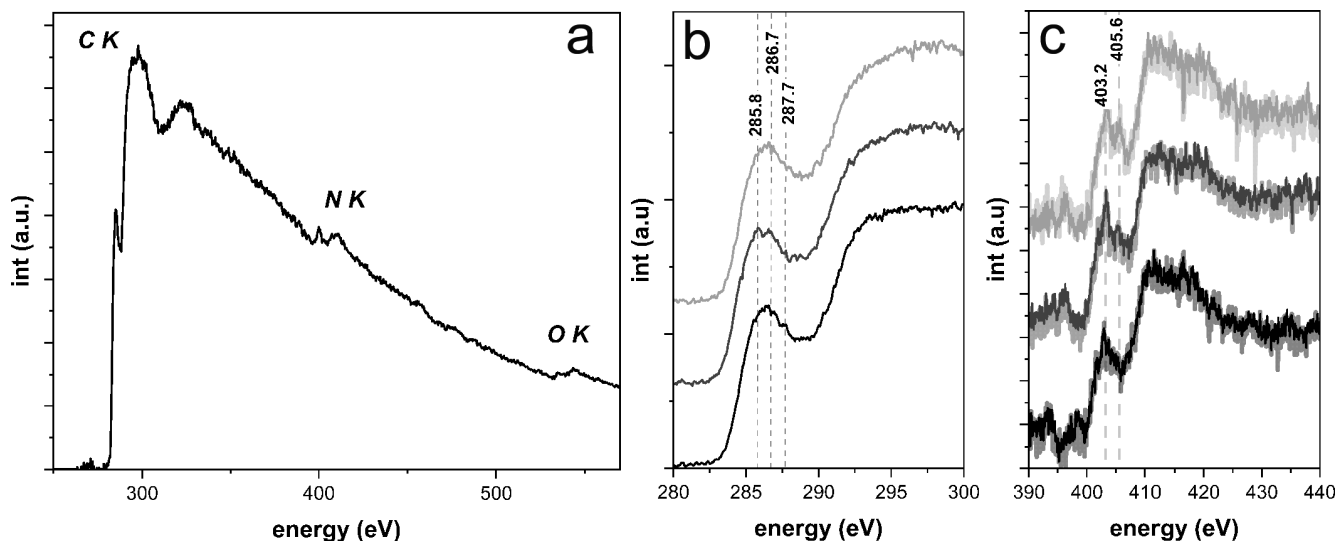


Fig. 9. EEL spectra of different regions within grain B7\_1b. a) Overview spectrum with a large energy dispersion that shows the three major element edges. b) C-K edge spectra within region #3 of the grain (see Fig. 7). The major fine structure on top of the  $\pi^*$  edge is the band at around 286.6 eV from ketone and/or aldehyde bonding with some possible nitrile contribution as well as some aliphatic bonding at around 287.7 eV. c) N-K edge of the same region #3 within the grain, denoised by PCA and plotted with darker color over the raw spectra. The major absorption at around 403.2 eV due to amine or amide bonding as well as possible fine structure at around 405.6 eV due to possible nitro groups can be identified.

weakly metamorphosed chondrites, where the intensity ratios of the D- to the G-band ( $I_D/I_G$ ) increase with increasing thermal metamorphism. It is also compatible to what has been measured by Raman spectroscopy on extracted bulk IOM of Renazzo, which showed an  $I_D/I_G$  ratio of  $0.93 \pm 0.07$  (Quirico et al. 2014). However, there is no straightforward relationship between that ratio and structural order, and it is discussed already by Bonal et al. (2007) that especially in poorly ordered amorphous OM, other factors such as time, chemistry, and pressure play an important role for OM maturation.

In spite of the current limitations in energy resolution and the lack of straightforward comparison to optical data, the strength of the STEM-EELS approach lies in the greatly enhanced spatial resolution and sensitivity. It is well known that vibrational modes can be excited from afar. The so-called “aloof beam” geometry, whereby the beam is positioned in the vacuum close to the sample, exploits the fact that the signal is then dominated by long-range dipole excitations to avoid beam-induced damage, although even in aloof beam mode, some level of spatial sensitivity is retained (Haiber and Crozier 2018). Here, the measurements were performed in impact mode, that is, with the beam placed on the sample to directly correlate the vibrational response to the earlier core loss analysis. In this geometry, locally excited modes are a strong contributor to the total recorded intensity. Measurements performed on metal-organic materials, using experimental conditions very similar to the results presented here,

have recently shown that distinct vibrational modes can be identified with spatial sensitivity better than 10 nm (Collins et al. 2019). We therefore expect that the spectral variations from the OM observed here are strongly correlated with the local functionality.

The observation of vibrational bands associated with specific functional chemistries from the very same sample location used for analytical electron microscopy can serve as an unambiguous confirmation that the functional groups are still intact, in spite of the challenging sample preparation procedure. Furthermore, very recent progress in the field made it possible to distinguish site-specific  $^{12}\text{C}/^{13}\text{C}$  isotopic labels in L-alanine crystals with nanometer spatial sensitivity (Hachtel et al. 2019) providing further exciting prospects for the use of this technique in the study of anomalous organic hotspots. Future work on other meteoritic OM with known Raman and IR properties to compare to obtained low-loss spectra such as here is clearly necessary and could provide important clues about the sub-nm complex evolution of OM.

## DISCUSSION

### Implications from Morphologies and Petrographic Context

The morphologies of organic grains in extraterrestrial samples can give important clues about their formation mechanisms. Recent “in situ”

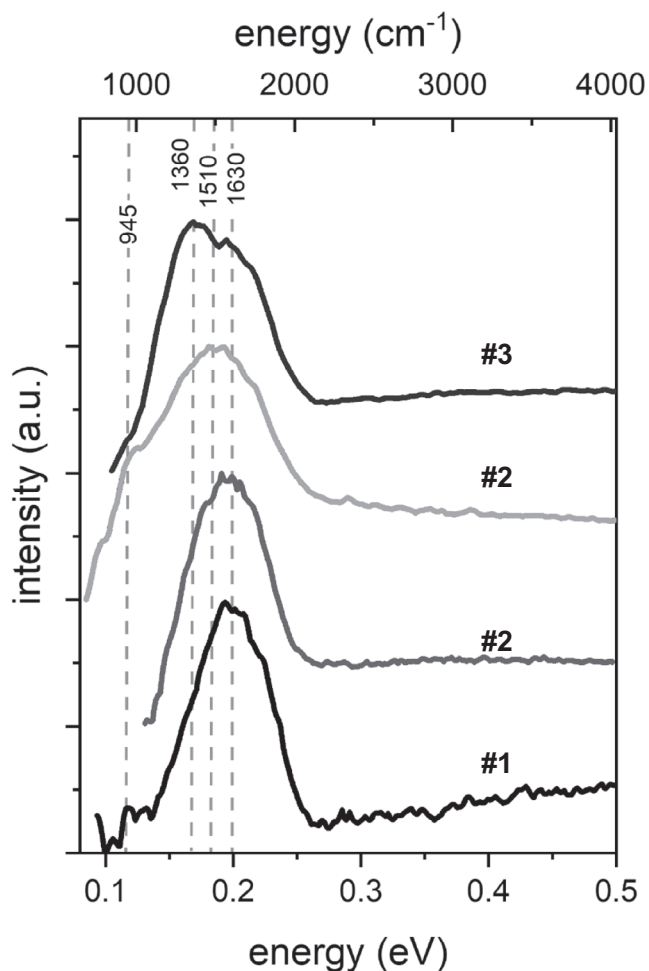


Fig. 10. Low loss (vibrational) electron spectroscopy with very high energy resolution obtained on different regions within grain B7\_1b indicated by #1-3 in Fig. 7. The two major bands at around 1360 and 1630  $\text{cm}^{-1}$  can be identified, which most likely relate to the D- and G-bands of polyaromatic hydrocarbons known from Raman spectroscopy. Additional vibrational intensity from C=C and C-O stretch modes known from infrared spectroscopy may also contribute to the observed peaks. However, peak positions on different regions within the grain vary on a nanometer scale, most likely due to the heterogeneous nature of the organic matter.

investigations have generally shown that the OM can be morphologically and petrographically extremely complex on a nanometer scale. It can occur either as diffuse regions distributed throughout the meteorite or IDP matrix, or as well-defined rounded or globular objects separated from the surrounding components (Nakamura-Messenger et al. 2006; Le Guillou et al. 2014; Vollmer et al. 2014; Changela et al. 2018). Some investigations indicate that diffuse OM seems more abundant in cometary samples such as chondritic-porous or ultra-carbonaceous IDPs (Matrajt et al. 2012) whereas the better defined globular OM is more common in

meteoritic matrices that have experienced mild aqueous alteration. In the following, we want to discuss these opposing views related to the complex OM morphologies observed here.

In chondritic-porous IDPs, as well as in certain porous AMMs, it has been found that the OM mainly consists of a diffuse submicron material. It often occurs as rinds on grain surfaces, which glue together larger minerals such as silicates and sulfides (Flynn et al. 2003; Keller et al. 2004; Matrajt et al. 2012; Noguchi et al. 2017; Yabuta et al. 2017). Because it is generally accepted that the parent bodies of most IDPs and AMMs represent comets from the outer solar system beyond the snow line (Nesvorný et al. 2010), aqueous alteration of these particles is assumed to be minimal (e.g., Berger et al. 2011). This OM most likely consists of very small ( $\ll 100$  nm) subunits that have formed either in circumstellar or interstellar environments or by irradiation of icy particles in the early solar nebula. Therefore, they represent some sort of starting material in the early solar nebula from which the OM that we find today may have evolved.

Interestingly, in more altered CR1 chondrites, such as GRO 95577, as well as the CM2 Murchison and the CI1 Orgueil, a similar diffuse organic component has been described (Le Guillou et al. 2014; Vinogradoff et al. 2017; Changela et al. 2018). The genetic connection between these two types of diffuse organic compounds is unclear at the moment. It has been argued that the diffuse OM in more heavily altered type 1 chondrites may be the result of breakdown reactions from the more globular OM, in a similar manner as in terrestrial shale maturation reactions (Changela et al. 2018). As the parent bodies of cometary IDPs and processed CR chondrites are clearly different and have experienced distinct alteration histories, understanding the origins of this diffuse OM in these parent bodies and whether it represents a more pristine, or a more altered organic material, is key to understanding the evolution of OM. It is therefore important to investigate these two types of diffuse OM in more detail by comparative studies on IDPs and CMs. However, a major drawback in such comparative studies is that the information length scales are usually vastly different, because IDP OM can only be investigated by high spatial resolution techniques, whereas meteoritic OM can be extracted by solvents as bulk samples. In CRs, it has been observed that the diffuse OM more likely occurs in close association with nano-phyllsilicates and amorphous silicates than with crystalline silicates or sulfides (Changela et al. 2018). In IDPs, however, it is associated with all kinds of crystalline and noncrystalline materials, and it is therefore unclear at the moment whether these noncarbonaceous materials



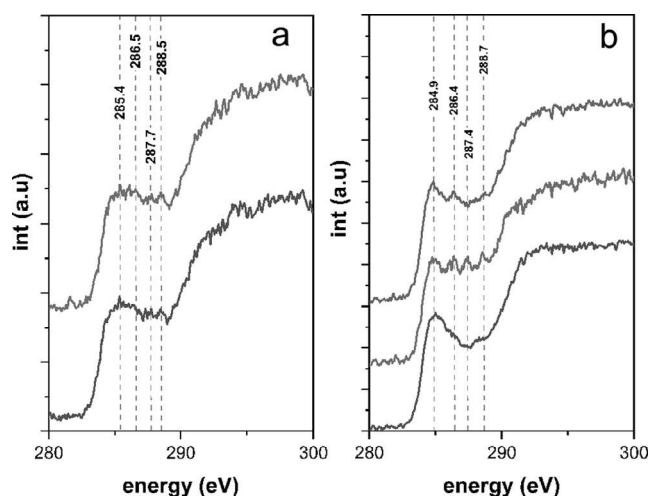


Fig. 11. Carbon K-edge EEL spectra on different regions within extracted grains OM4 and OM166, where no nitrogen could be identified. The EEL spectrum of grain OM4 (a) acquired in the region marked in Fig. 7 shows weak evidence for ketone/aldehyde (286.5 eV), aliphatic (287.7 eV), and carboxylic (288.5 eV) bonding, which has been observed in other XANES work on diffuse OM as well (Changela et al. 2018); OM166 (b) shows a heterogeneous distribution of different functional groups (spectra taken in region #2 marked in Fig. 6), with sometimes strong absorption only at the 285 eV band (lower spectrum), but also regions where all four characteristic functional groups present in meteoritic OM can be observed (middle spectrum). In the middle spectrum, Ca has been observed as well (not shown).

have played a role in catalytic modifications of OM in IDPs.

To summarize, there are apparently at least two types of diffuse OM present within primitive extraterrestrial samples, whose origins are not well constrained. This diffuse component is present among the OM regions investigated here (e.g., Fig. 1: OM196, Figs. 2 and 7: OM4), but was not the focus of our TEM investigations, and we did not specifically aim at these diffuse OM particles for FIB preparation. Clearly, even among the more globular and better defined particles that we did target for TEM analysis, some diffuse OM component was still present on a nanometer scale such as in grain OM4. This close morphological association of diffuse OM with the more globular OM strongly argues for a genetic connection between these two types of OM. Because the diffuse OM is generally not the major target for FIB preparation, their high spatial resolution investigations are still in their infancy, and more information concerning its functional chemistry and morphologies is urgently needed.

A second morphologically distinct organic component has been identified in IDPs, AMMs, and Wild 2 samples (Nakamura-Messenger et al. 2006; De Gregorio et al. 2010; Noguchi et al. 2017) as well as in differently altered

CI, CR, and CM chondrites (Garvie and Buseck 2004; Le Guillou et al. 2012; De Gregorio et al. 2013). Initially, this component had been termed “nanoglobules,” because it occurs as very small, roundish objects, but it has been shown in follow-up studies that these particles can be morphologically quite diverse. Sometimes these globules surround mineral grains or fragments such as possibly in grain OM211 here (Fig. 3), but it is also very common that they simply occur as globular grains with no apparent central feature. Furthermore, it has been shown that this globular OM can also aggregate to even larger distinct objects that cannot be termed “nanoglobules” anymore but rather “microglobules” or “globule clusters,” such as in the Renazzo grains studied here or in other CR and CM chondrites (Le Guillou et al. 2014; Hashiguchi et al. 2015; Changela et al. 2018).

The origins and evolution of this enigmatic component are still controversial. Because such globules have been found in IDPs, Wild 2 material, and some AMMs that likely have escaped severe aqueous modification, it was initially accepted that they must represent highly pristine molecular cloud or outer solar nebula objects or even grains from circumstellar and interstellar environments (Nakamura-Messenger et al. 2006; Saito and Kimura 2009). This was also based on their occasionally highly anomalous isotopic compositions. However, other work argues that it is possible to synthesize such globular grains by reactions in an aqueous solution and enhanced temperatures (Cody et al. 2011; Kebukawa et al. 2013) and that some of these objects might therefore also form on respective asteroidal parent bodies. Our results suggest that for the multiglobular and layered OM grains in Renazzo investigated here, an alteration scenario on the meteorite parent body is more likely. The organic layers often alternate with noncarbonaceous mineral layers (silicates and sulfides, Fig. 8) in a highly pronounced texture, and this mineralogical observation is difficult to explain by irradiation reactions in a nebular environment. This texture has not been previously observed in other TEM work on Renazzo (Le Guillou et al. 2014), where OM morphologies are described as “aggregates,” but not as the layered mantles found here. We infer that this prominent petrographic texture can only be explained by exposition of material to fluids with strongly varying chemical compositions and cation activities on a micrometer scale. It is known from other work on meteorite aqueous alteration, for example, on so-called “tochilinite-cronstedtite-intergrowths” in CM chondrites (e.g., Pignatelli et al. 2016) that alteration conditions and fluid compositions on meteorite parent bodies varied drastically over time leading to alternating nanometer-sized sulfide and silicate mineral layers. It is therefore straightforward to argue that similar fluids

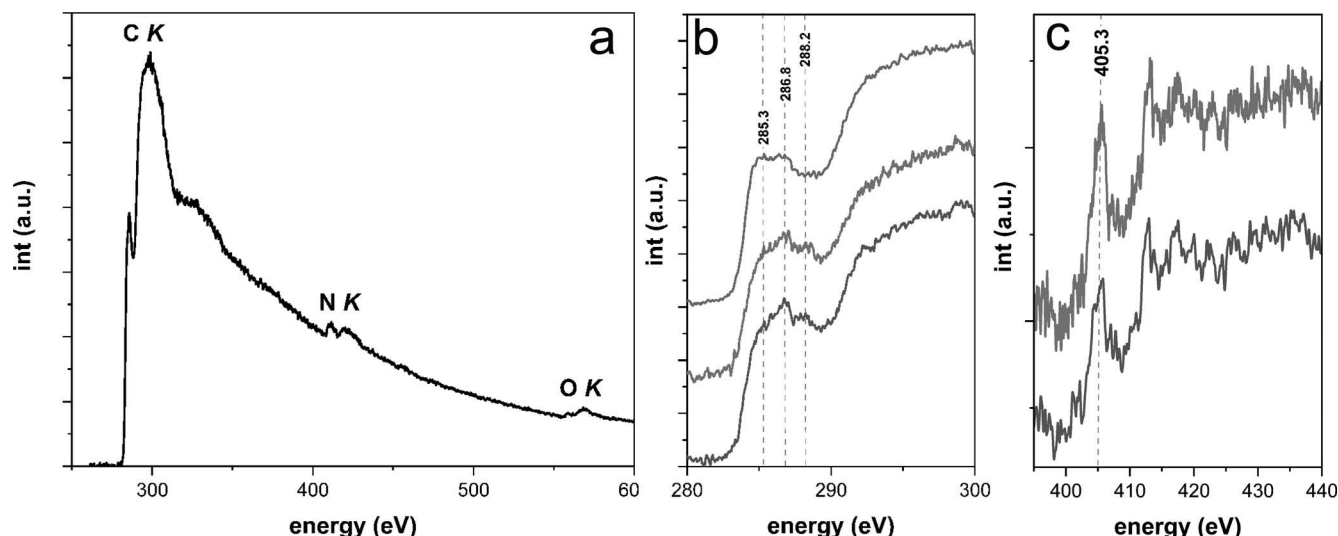


Fig. 12. EEL spectra of different regions within grain OM164 indicated in Fig. 6 by #1+3. a) Overview spectrum with a large energy dispersion that shows the three major element edges. b) C-K edge spectra of region #3 within the grain. The major fine structure on top of the  $\pi^*$  edge are the bands at around 286.7 eV from ketone/aldehyde/nitrile bonding and at 288.2 eV due to carboxylic bonding. c) N-K edge of region #1 within the grain (raw data). The spectra are very noisy due to the very low N abundance, with major absorption at around 405 eV due to possible nitrate groups present in analyzed regions.

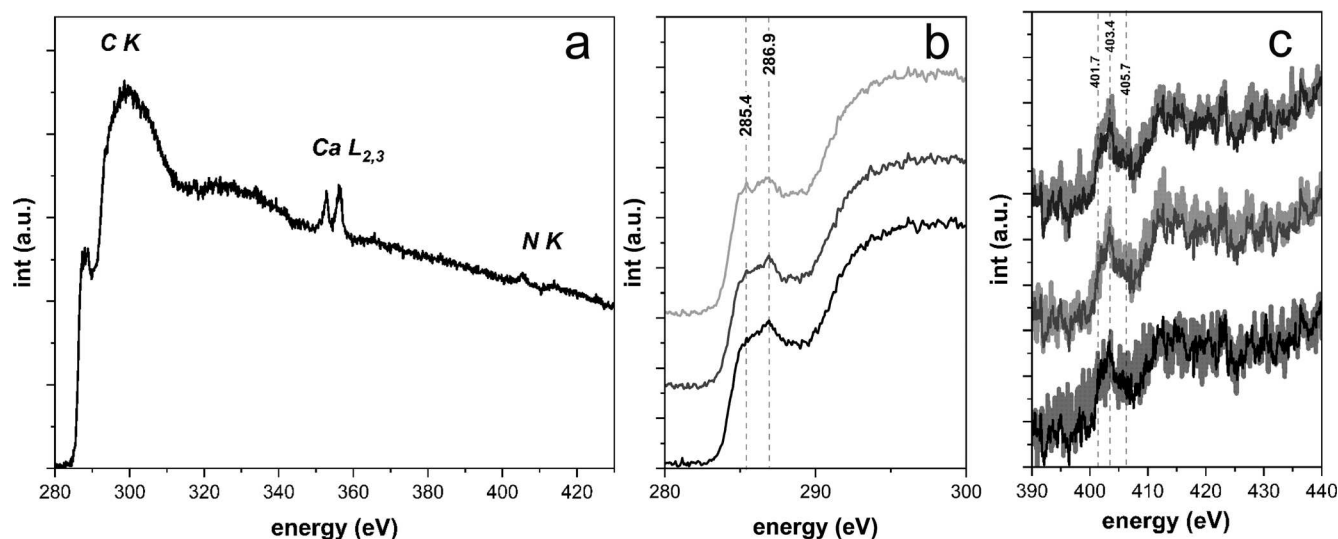


Fig. 13. EEL spectra of different regions within grain OM210 indicated in Fig. 6 by #2+3. a) Overview spectrum with a large energy dispersion that shows the two major element edges as well as dominant Ca-L edges. b) C-K edge spectra within region #2 of the grain, where no nitrogen was detected. The major fine structure on top of the  $\pi^*$  edge is the band at around 286.9 eV from ketone/aldehyde bonding. c) N-K edge of region #3 within the grain, denoised by PCA and plotted with darker color over the raw spectra. The spectra are very noisy due to the very low N abundance, with some absorption at around 401.7 eV due to amidyl-N, major absorption at around 403.4 to most likely nitro bonding, and very weakly at 405.7 eV due to possible nitrate groups present in analyzed regions.

might also have modified abundant organic molecules. The exact conditions of these alteration reactions are difficult to infer from our observations alone.

Globular organics in this work as well as in other work are also often intimately associated with carbonates, halogenides, or pure Ca on a nanometer

scale (Le Guillou et al. 2014; Vollmer et al. 2014; Vinogradoff et al. 2017; Fig. 13: OM210), which represent typical fingerprints of aqueous reactions and again supports the parent body scenario. The observation here that the OM often fills up cracks within the porous matrix of the brecciated chondrite

Table 2. Overview of characteristics of FIB-extracted grains.

Grain	$\delta^{15}\text{N}$	Size	Element ratios	Notes
REN_B7_1b	$500 \pm 10\%$	$\sim 0.5 \times 1 \mu\text{m}$	N/C $\sim 0.1$ , O/C $\sim 0.9$	Two grains, strong N-K edge
REN_OM4	$410 \pm 10\%$ (bulk)	$\sim 50\text{--}200 \text{ nm}$	N < D.L.	Oval globules dispersed, sheet silicate encapsulation
REN_OM164	$770 \pm 10\%$ (bulk) $1040 \pm 10\%$ (hotspot)	$\sim 4 \times 10 \mu\text{m}$	N/C $\sim 0.07$ , O/C $\sim 0.07$	
REN_OM166	$200 \pm 10\%$ (bulk) $720 \pm 40\%$ ( $^{15}\text{N}$ -rich layer) $131 \pm 19\%$ (outer shell)	$\sim 4 \times 4 \mu\text{m}$	N < D.L.	Ca detected
REN_OM210	$880 \pm 10\%$ (bulk) $530 \pm 10\%$ (high-D-layer) $1670 \pm 10\%$ (outer shell)	$\sim 3 \mu\text{m}$	N/C $\sim 0.03$	Heterogeneous N distribution, Ca detected

Renazzo, as observed in other studies, also strongly supports a late-stage modification scenario.

We do not see any correlation between C-N isotopic compositions and morphologies of the Renazzo grains in this study. This would seem difficult to reconcile with the parent body scenario, because then we would expect that anomalous nitrogen isotopic compositions would be modified or diminished as suggested for diluted presolar grain isotopic compositions. However, here we strongly argue for a fluid being enriched in  $^{15}\text{N}$  (see below), which acts as a modification agent leaving the isotopic composition unaffected (or at least not completely erased). This has important implications for future investigations on OM, because then the mere existence of a  $^{15}\text{N}$  anomaly does not necessarily mean that the grain represents unaffected molecular cloud material.

The importance of hydrous reactions on the constitution of OM has also been confirmed in several studies, initially by bulk analyses of extracted soluble components (e.g., Glavin and Dworkin 2009; Pizzarello and Shock 2017), bulk analyses of IOM (e.g., Alexander et al. 2007), and more rarely by in situ studies (e.g., Le Guillou et al. 2014; Vollmer et al. 2014). The apparent contradiction concerning the origins of globular organic grains is difficult to reconcile with our current knowledge. It is therefore possible that there are two types of organic nanoglobules present within extraterrestrial samples, that is, a pristine one from molecular cloud or nebular origins, and a more evolved one formed by parent body reactions. Irradiation of icy mantles rich in simple organic molecules may lead to the synthesis of more complex organics with globular textures, as has been proposed in numerous studies (e.g., Dartois et al. 2005; Nakamura-Messenger et al. 2006; Ciesla and Sandford 2012), but a globular appearance might as well be the result of exposure to an aqueous fluid within a porous asteroidal body such as in this work. Morphologically, these two types of

nanoglobules are apparently quite similar, and it seems plausible that both types of mechanisms might have played a role in their evolution. The occurrence of OM as (nano/micro)globular objects is obviously a widespread phenomenon in the early solar system, because these types of grains occur in a wide variety of extraterrestrial samples with completely different histories. It is a speculative but exciting possibility that these particles might have played an important role for early forms of pristine prebiotic molecules, because their roundish, globular appearance might have served as scaffolds for very early cell membranes (Ehrenfreund et al. 2006).

Summarizing our discussion on morphological varieties of Renazzo OM, it can be stated that the globular and multiglobular/layered textures dominate over the more diffuse ones, which is likely due to parent body fluid reactions even for the ones that are isotopically anomalous in nitrogen. We do not see any correlation between morphologies and C-N isotopic compositions of the OM grains in this study. Furthermore, the OM is often aggregated into larger particles several micrometers in size, and often occurs along cracks within the meteorite. These morphological observations as well as textural relationships between the meteoritic OM and alternating mineral layers and the surrounding matrix strongly argue for alteration and modification reactions of respective organic grains, but not necessarily formation on the meteorite parent body.

### The Response of Functional Chemistry to Possible Formation Scenarios

#### *C-K Edge Functional Chemistry*

There is growing evidence from EELS and STXM analyses on OM that the diffuse and globular types of meteoritic and cometary OM as described above can be roughly distinguished by certain enrichments or



depletions of functional groups within the macromolecular kerogen. The bulk of extracted IOM from diverse meteorite samples is characterized by three distinct absorption bands due to aromatic/olefinic, ketone/aldehyde/phenol, and carboxylic functional groups as fine structure on the main  $\pi^*$  and  $\sigma^*$  C-K edge absorption features (e.g., Cody et al. 2008; De Gregorio et al. 2013). However, the relative abundances of these different functional groups vary from one sample to another, and also within a given sample on a nanometer scale, which has been demonstrated by in situ methods such as STEM-EELS and STXM. However, such analyses limit the total number of distinct particles that can be analyzed and thus may not be representative compared with bulk extraction analyses, which provide a more global picture of functional chemistry. Still, from the bulk analysis of IOM alone, it is often not possible to draw tight conclusions about possible formation pathways of this complex material, so complementary high spatial resolution techniques as deployed here are essential.

Additional bands to this “IOM-like” signature at the C-K edge (De Gregorio et al. 2013) are mostly due to aliphatic bonding at around 287 eV as well as a carbonate peak at 290.3 eV in some samples. It has been postulated that a higher fraction of aliphatic versus aromatic domains might be indicative of more pristine OM, because this has been observed in cometary IDP organics (Flynn et al. 2003; Keller et al. 2004; Vollmer et al. 2014). However, in more altered chondrites like the CR1 GRO 95577, the apparently more altered and diffuse OM component also exhibits a more aliphatic, as well as a more carboxylic, functional chemistry. This process has been compared to terrestrial shale maturation, where smaller soluble (bitumen-like) fractions can be released from complex kerogens as more aliphatic and carboxylic molecules leaving a more aromatic residue behind (Changela et al. 2018).

The “IOM-like” signature at the C-K edge described above as well as aliphatic bonding occurs in the OM grains of our study as well (Figs. 9, 11–13). However, intensities of these bands vary on a nanometer scale, even within the same grain. This is in contrast to the work of Le Guillou et al. (2014), who analyzed functional chemistry of Renazzo organics by STXM methods and do not observe any internal chemical heterogeneities but rather a homogeneous chemical (“IOM-like”) signature. This attests to the fine-grained chemical complexity of meteoritic organics that can be averaged out by the wider synchrotron beam compared to the sub-nm electron beam in the TEM. For example, within grain OM166 (Fig. 11b), we observe indication for both strong aromatic

hydrocarbons (lower spectrum in Fig. 11b) as well as for “IOM-like” and aliphatic bonding (middle spectrum in Fig. 11b). The same is true for grain B7-1b, which also shows indication for both functional chemistries (Fig. 9b). We therefore do not observe any strong correlation between morphology and functional chemistry; globular grains may contain less aromatic domains (e.g., grain B7-1b, Fig. 9b), whereas grains with a diffuse appearance like OM4 turn out to contain globular subunits upon closer scrutiny (Figs. 7 and 11).

It has been suggested that the functional chemistry of the more globular, well-defined OM within meteorite samples is generally characterized by a higher abundance of aromatic, polymerized rings, indicated by the relative height of the  $\pi^*$  peak at around 285 eV compared to the total carbon content (Vinogradoff et al. 2017) as well as distinct absorption at around 286.5 eV due to C-O bonding (aromatic ketone/aldehyde or nitrile). It has been argued that the higher aromaticity of this globular component could be due to pre-accretionary irradiation and loss of aliphatic groups in molecular cloud or nebular environments, and there are indications that proceeding aqueous alteration in chondrites may then decrease observed aromaticity again (see discussion by De Gregorio et al. 2013). However, it has also been proposed that this functional chemistry signature can be produced by the formose reaction on meteorite parent bodies by aqueous alteration (Cody et al. 2011). Based on the widespread occurrence of globular organics in all types of extraterrestrial samples (see above), no tight conclusions can be drawn concerning their origins and it may form by a variety of different mechanisms (De Gregorio et al. 2013). In our work, we observe the presence of the aromatic 285 eV peak within all organic grains analyzed by EELS, however, with varying intensity even within the same grain. This supports the conclusion that the morphology and the functional chemistry at the C-K edge, specifically the strength of the aromatic feature, cannot be assigned to any certain formation process.

The occurrence of Ca and a carbonate peak within the C-K absorption edge fine structure in OM in different samples can be used as a more reliable fingerprint of fluid reactions, but this carbonate bonding is only rarely observed. For example, there is evidence from C-XANES spectra of the aqueously altered chondrites Orgueil (Garvie and Buseck 2006), and Tagish Lake (Zega et al. 2010) for carbonate bonding as well as in some CR chondrites such as Al Rais (Le Guillou et al. 2014), OM in a clast from the H3-6 Zag chondrite (Kebukawa et al. 2019). In this work, evidence of Ca was only found in grain OM210 (Fig. 13). Interestingly, even some IDPs contain such a carbonate bonding peak or even only pure Ca (Flynn

et al. 2003; Vollmer et al. 2014), which demonstrates that even the theoretically “dry” cometary parent bodies might have experienced some mild aqueous reactions in some parts. Furthermore, the carbonate or Ca bonding is not necessarily associated with distinct calcite grains within the OM, so it has been suggested that it is bonded to the OM itself and later serves as an agent to precipitate carbonate crystals.

We are therefore left with the following qualitative reaction pathway combining morphological and functional chemistry observations: pristine organics in IDPs and AMMs have not experienced any severe aqueous alteration and may be composed of a less aromatic, more aliphatic kerogen. Pre-accretionary irradiation may then lead to a more pronounced aromaticity of that OM by polymerization reactions in carbon-rich ices. However, subsequent subtle aqueous alteration on meteorite parent bodies may lead to morphological changes and to larger and aggregated organic particles with an even more aromatic signature as observed in the more altered regions of different CR chondrites (e.g., Changela et al. 2018). However, when alteration becomes more severe such as in CR1 or CM chondrites, this OM evolves to a diffuse material with again smaller, and more aliphatic and carboxylic bonding due to breakdown reactions. This again underlines the complexity of OM evolution and stresses the need for more in situ work in this respect.

### *N-K Edge Functional Chemistry*

Further information can be gained through the analysis of the nitrogen functional chemistry of extraterrestrial OM. However, these investigations are much rarer compared to analyses on the C-K edge, because of the low abundance of nitrogen within these samples (atomic N/C ~0.1). Even by synchrotron techniques, N-K edge spectra are usually very noisy (e.g., Cody et al. 2008) and difficult to interpret. Very often, the N-K edge is not observed at all, although previous NanoSIMS analyses have shown the presence of high N/C ratios. The scarcity of a strong N-K edge has been interpreted by the fact that this component seems very prone to destruction and alteration, either already on the parent body or by analytical techniques, for example, by ion or electron irradiation.

In some organic grains, strong absorption bands at around 400 eV were linked to a likely high abundance of C-N double and triple bonding environments (imine and nitrile; Busemann et al. 2007; Vollmer et al. 2014). Furthermore, in less altered carbonaceous chondrites such as the CR2 chondrite QUE 99177 or in ultra-carbonaceous AMMs, the IOM also exhibits prominent absorption below 400 eV due to these bonding environments (Alexander et al. 2017; Yabuta et al.

2017). However, Cody and Alexander (2017) noted that such bonding environments, especially triply bonded nitrile, are very prone to alteration and modification, and unlikely to survive in meteoritic OM upon aqueous alteration reactions. This might explain why we do not see indication for these functional groups in the organics of the more altered chondrite Renazzo studied here. In that work, synchrotron XANES has been used to fit a multitude of spectra at the N-K edge of the pristine chondrite Tagish Lake, shown to contain highly primitive organics (Herd et al. 2011). It was shown that the spectra can be fitted by a contribution of only little imine and nitrile functional groups (3–4%), whereas the majority is accounted for by N-heterocycles such as pyrrole (C<sub>4</sub>H<sub>4</sub>NH) as well as secondary (R-NH-R) and tertiary (N-R<sub>3</sub>) amines. It is noted, however, that a large fraction of the IOM signal in N-K edge XANES spectra of Tagish Lake cannot be fitted by those functional groups alone, and it is argued that a high abundance of nitro groups, for example, oxygenated N-rich functional groups (NO<sub>2</sub>-), would explain the absorption spectra as a whole. If we apply these arguments to analyzed bands in N-K edge spectra here, we can make the following observations. OM particles without a strong N-K edge signature such as OM4 and OM166 (Fig. 11) are also characterized by carboxylic bonding environments in C-K edge spectra, at least in some areas of these grains. It can therefore be argued that these particles have experienced more severe aqueous alteration that has led to a destruction of C-N bonds and the formation of more pronounced COOH-bonding as a by-product of these reactions. This is in agreement with observations by Changela et al. (2018), who see an increase in carboxylic functional chemistry in the more altered, diffuse regions in CR chondrite OM. Interestingly, in spectra of grains with a pronounced N-K edge signature such as B7-1b and OM210 (Figs. 9 and 13), we do not observe any absorption at the 288 eV carboxylic band. We therefore support the conclusion that a higher abundance of carboxylic functional groups within meteoritic OM is an indicator of more advanced aqueous alteration reactions that have likely also destroyed N-K edge functional chemistry within these grains.

The OM particles with observed N-K edge functionality such as OM210 and B7-1b also show strong absorption at the aromatic 285 eV as well as at the ketone/aldehyde 286.6 eV band. This might be an indicator that increased aromaticity together with pronounced N-K edge chemistry are coupled, which could be due to certain polymerization reactions such as the formose synthesis (see below). However, in grain OM164, the aromatic signature is again decreased, whereas the noisy N-K edge spectra only show

absorption at the 405.3 eV nitrate band, which is very likely due to oxygenation reactions. This grain also shows carboxylic bands at the C-K edge, which again supports the conclusion drawn above. The least altered OM in this respect is therefore represented by grain B7-1b, which still shows some aliphatic bonding as an indicator of more pristine organics such as found in IDPs as well as very strong aromatic bonding and pronounced amine/amide N-K edge functional chemistry with almost no bands of oxygenated nitrogen. Grain OM210, which is apparently more altered, shows weak amidyl bonding, but also significant signs of more oxygenated nitrogen groups such as nitro and nitrate bonding.

We can therefore summarize our observed evolution of N-K edge functional chemistry as follows (although this analysis is clearly based on a very limited number of grains): OM grains with relatively high N/C ratios also show indication for strong aromaticity, ketone/aldehyde bonding, and less carboxylic functional groups, together with indications for amide/amine functional chemistry at the N-K edge. With more advanced alteration, carboxylic functional groups appear, and N-K edge functionality becomes more oxygenated indicated by the presence of nitro and/or nitrate groups. At the final stage of these alteration reactions, nitrogen cannot be detected anymore within these organic grains. Clearly, the database to interpret N-K edge functionality is still in its infancy and more work is desperately needed.

### **Synthesis: Origins of Complex Layered Morphologies, Heterogeneous Isotopic Compositions, and Functional Chemistry Observations**

The origins of nitrogen isotopic anomalies within OM are still not well constrained. It is either possible that they form in response to low-temperature fractionation reactions (Terzieva and Herbst 2000; Charnley and Rodgers 2002; Aléon 2010; Wirström et al. 2012), but it is also likely that they evolve in the inner solar nebula via selective photodissociation reactions in response to UV irradiation, analogous to the well-studied oxygen isotope fractionation self-shielding model (Muskatell et al. 2011; Chakraborty et al. 2014; Füri and Marty 2015). One argument against the low-temperature model is the fact that observed  $^{15}\text{N}$  enrichments in interstellar or molecular clouds are much higher than expected from theoretical considerations. Furthermore and supporting the irradiation theory,  $^{15}\text{N}$  enrichments of  $\sim 12,000\%$  were produced experimentally by 90 nm UV radiation of an  $\text{N}_2\text{-H}_2$  mix (Chakraborty et al. 2014), and very recent modeling also supports the self-shielding hypothesis

(Visser et al. 2018). In any case, the survival of such  $^{15}\text{N}$  anomalies in OM is evidence that any severe later overprint has not occurred. Thermal metamorphism or extensive aqueous alteration would erase isotopic anomalies similar to nucleosynthetic anomalies of presolar grains, because they are much less abundant in thermally metamorphosed petrologic types 4–6 or heavily altered type 1 chondrites.

Heterogeneous  $^{15}\text{N}$ -anomalous compositions of OM have been observed in other in situ studies, for example, in IDPs (Floss et al. 2004, 2006; Keller et al. 2004) and meteorites (Busemann et al. 2006; Kebukawa et al. 2019). In some cases, this apparent heterogeneity might be explained partially by statistical scattering within small regions of interest, but in the Renazzo grains studied here, these vastly different isotopic compositions are clearly distinct within NanoSIMS errors (Tables 1 and S1). As mentioned above, the multiglobular texture of these grains with intermingled sheet silicates as clearly defined layers between the organic grains (Figs. 7 and 8) is unlikely to have occurred by a nebular process. This would more likely lead to a statistical mixture of materials on a much finer scale such as in the surrounding meteorite matrix, where presolar grains and aqueously altered minerals occur directly next to one another. It rather attests to parent body reactions under varying chemical conditions (Si or S activity, elemental ratios, pH, water:rock ratios). Such spatially and temporally changing “microchemical” environments have been traditionally invoked to explain the occurrence of differently altered minerals within aqueously altered meteorites on micrometer or even submicrometer scales (Brearley 2006).

We argue here that our observed layered distribution of  $^{15}\text{N}$ -anomalous OM underlines the importance of fluids to redistribute organics, while retaining their anomalous signatures. It has been observed experimentally that  $^{15}\text{N}$ -anomalous ammonia can be released from OM in chondrites upon hydrothermal treatment (Pizzarello and Bose 2015), and can then be redistributed as an agent for other, complex synthesis reactions within the parent body. A prominent example for such a reaction is represented by the Strecker-cyanohydrin synthesis, where the presence of ammonia is an important prerequisite to form  $\alpha$ -amino acids from precursor carbonyl (aldehyde/ketone) compounds (Simkus et al. 2018). It is puzzling, however, that this releasable ammonia within the meteoritic IOM should have survived the harsh acid treatment used to produce the IOM extracts in the first place, although this could be due to the specific bonding environment of this ammonia (Pizzarello and Bose 2015).

The evolution of this organic component is summarized as follows according to that work:  $^{15}\text{N}$ -



enriched ammonia would form during these nebular stages by UV irradiation of  $N_2$  and  $H_2$  condensed mixtures (Chakraborty et al. 2014; Pizzarello and Bose 2015). Ammonia is also well known to occur in a variety of astrophysical and solar system environments, such as comets (Wyckoff et al. 1991; Goesmann et al. 2015) or the surface of the dwarf planet Ceres (King et al. 1992; De Sanctis et al. 2015). It also forms efficiently with enhanced  $^{15}N/^{14}N$  ratios in dense molecular clouds and rapidly accretes into ice particles (Charnley and Rodgers 2002). During incorporation into the meteorite parent bodies, this anomalous ammonia then plays an important role in proceeding organic synthesis reactions. One example is the Strecker synthesis scheme mentioned above, and a further case is represented by the formose reaction invoked by Cody et al. (2011) to polymerize formaldehyde molecules to polycyclic aromatic hydrocarbons. It has been shown experimentally that this formose reaction does not proceed at low temperatures in the absence of ammonia, but that the presence of small traces of this molecule ( $NH_3/H_2CO \geq 0.005$ ) already induces the synthesis of a considerable fraction of the initial formaldehyde into more complex organics (Schutte et al. 1993).

To summarize our observations on heterogeneous  $^{15}N$ -anomalous organics in Renazzo in combination with arguments discussed in other work on  $^{15}N$  isotopic compositions, we suggest here that the carrier phase of  $^{15}N$ -enrichments of meteoritic OM is best represented by ammonia formed in the solar nebula or the parent molecular cloud. This component was later redistributed by mild aqueous reactions on asteroidal parent bodies and aided in the formation of more complex, polyaromatic kerogen molecules via Strecker-type or formose reactions. We therefore propose that the detection of variable  $^{15}N$  enrichments in meteoritic OM is an ambiguous indicator of extreme primitiveness, as this observation can as well attest to proceeding redistribution and chemical reactions evolving from pristine simple organic molecules on meteorite parent bodies.

## CONCLUSIONS

We have investigated the textures, morphologies, isotopic compositions, and functional chemistries of organic grains in the Renazzo carbonaceous chondrite by combined high spatial resolution techniques (SEM–NanoSIMS–STEM–EELS). Our observations lead us to the following conclusions:

1. Textures and morphologies of organic grains are complex and diverse on a micrometer to nanometer

scale. Some grains occur as tiny, submicron, diffuse areas intermingled with silicate and sulfide material, other grains have infiltrated large cracks that extend over several microns in size. In some parts, organic grains occur as globular, agglomerated, micron-sized objects.

2. Some organic grains exhibit a quite distinct mineralogical texture, where layers of OM alternate with silicate and sulfide minerals. These “multiglobular” grains have varying sizes, and, to our knowledge, have not been documented yet in any other chondrite that prominently.
3. NanoSIMS analyses reveal that organic grains show C-N isotopic compositions that are within the range to what has been observed before, from a few hundred up to over a thousand per mil enrichments in  $^{15}N$ , whereas  $^{13}C$  anomalies are only moderate to absent. However, the layered “multiglobular” organics are characterized by heterogeneous  $^{15}N$  isotopic compositions, where areas with low enrichments alternate with layers of strong enrichments. This heterogeneous isotopic composition of organic grains lends strong support to recent suggestions that  $^{15}N$  anomalies of OM in primitive chondrites are the result of combined fractionation–parent body alteration processes.
4. STEM analyses of five electron transparent lamellae of selected,  $^{15}N$ -anomalous organic grains reveal that they mostly consist of amorphous, globular, distinct grains, well separated from the surrounding matrix. However, in some areas, we observe a close association with sheet silicates and an amorphous silicate groundmass. The “multiglobular” texture can also be observed on a submicron scale, where bands of tiny silicate and sulfide minerals crosscut respective organic areas.
5. Functional chemistry investigations by EELS reveal a chemical complexity of OM on a nanometer scale. However, all grains show strong absorption at the C-K edge at around 285, 286.6, 287, and 288.6 eV due to polymerized aromatic hydrocarbons and different carbon-oxygen (aldehyde, ketone, carboxyl) and aliphatic bonding environments. Nitrogen K-edge functional chemistry is as complex as carbon functionality, but we detect strong indications of amine or amide chemistry at around 402–403 eV with varying intensity as well as signs of N-heterocycles and oxygenated nitro and nitrate groups within the organic polymer. More altered grains are characterized by a decrease in nitrogen content, more oxygenated nitrogen functional chemistry, and the appearance of carboxylic functional groups.
6. We also performed ultra-low loss/vibrational spectroscopy in the TEM with very high energy

resolution ( $\Delta E = 0.01\text{--}0.02$  eV) on meteoritic OM. The observed vibrational modes match favorably with the D- and G-bands well known from Raman spectroscopy at around 0.17 and 0.2 eV energy loss on the tail of the zero loss peak with a relative ratio of about 1, similar to what has been observed before by Raman spectroscopy. Additional vibrational intensity from C=C and C-O stretch modes known from infrared spectroscopy may also contribute to the observed peaks. Future investigations of this signal could lead to further insight on meteoritic OM with a spatial resolution not achievable by conventional optical techniques.

7. The combined observation of (1) multiglobular layered organic aggregates, (2) heterogeneous  $^{15}\text{N}$ -anomalous compositions of these grains, and (3) indication of N-H<sub>x</sub> (amine) functional chemistry within some of these N-rich organic grains lends strong support to recent ideas that  $^{15}\text{N}$ -enriched ammonia (NH<sub>3</sub>), probably incorporated as ice particles in the solar nebula, was a powerful agent to synthesize more complex OM in aqueous asteroidal environments (Pizzarello and Bose 2015). It is therefore well conceivable that our observed complex  $^{15}\text{N}$ -enriched ammonia chemistry in Renazzo OM serves as an example for the formation of biorelevant molecules on meteorite parent bodies in general.

*Acknowledgments*—We thank Maren Müller and Michael Kappl at MPI for Polymer Research for FIB preparation, Elmar Gröner for technical support on the NanoSIMS, and Antje Sorowka (MPIC) for assistance with the SEM. C.V. and J.L. acknowledge support by the DFG through SPP1833 grants (VO1816/3-1, and LE 3279/2-1). The Renazzo thin section was kindly provided by Franz Brandstätter from the Natural History Museum in Vienna. SuperSTEM is the U.K. National Research Facility for Advanced Electron Microscopy, supported by the Engineering and Physics Science Research Council (EPSRC). H.B. has been supported by the Swiss SNF-funded NCCR “Planet S.”

*Editorial Handling*—Dr. Larry Nittler

## REFERENCES

- Abreu N. M. 2016. Why is it so difficult to classify Renazzo-type (CR) carbonaceous chondrites? — Implications from TEM observations of matrices for the sequences of aqueous alteration. *Geochimica et Cosmochimica Acta* 194:91–122.
- Aléon J. 2010. Multiple origins of nitrogen isotopic anomalies in meteorites and comets. *The Astrophysical Journal* 722:1342–1351.
- Alexander C. M. O’D., Fogel M., Yabuta H., and Cody G. D. 2007. The origin and evolution of chondrites recorded in the elemental and isotopic compositions of their macromolecular organic matter. *Geochimica et Cosmochimica Acta* 71:4380–4403.
- Alexander C. M. O’D., Cody G. D., De Gregorio B. T., Nittler L. R., and Stroud R. M. 2017. The nature, origin and modification of insoluble organic matter in chondrites, the major source of Earth’s C and N. *Chemie der Erde — Geochemistry* 77:227–256.
- Berger E. L., Zega T. J., Keller L. P., and Lauretta D. S. 2011. Evidence for aqueous activity on comet 81P/Wild 2 from sulfide mineral assemblages in Stardust samples and CI chondrites. *Geochimica et Cosmochimica Acta* 75:3501–3513.
- Blackmur M. S., Dumbill S., MacLaren I., Hernandez-Maldonado D., Styman P. D., Gass M., Nicholls R. J., Hyde J. M., Ramasse Q. M., Annand K. J., Smith J. S., and Gotham N. 2018. The association of hydrogen with nanometre bubbles of helium implanted into zirconium. *Scripta Materialia* 152:102–106.
- Bonal L., Bourot-Denise M., Quirico E., Montagnac G., and Lewin E. 2007. Organic matter and metamorphic history of CO chondrites. *Geochimica et Cosmochimica Acta* 71:1605–1623.
- Bradley J. P., Ishii H. A., Gillis-Davis J. J., Ciston J., Nielsen M. H., Bechtel H. A., and Martin M. C. 2014. Detection of solar wind-produced water in irradiated rims on silicate minerals. *Proceedings of the National Academy of Sciences* 111:1732.
- Brearely A. J. 2006. The action of water. In *Meteorites and the early solar system II*, edited by Lauretta D. S. and McSween H. Y. Jr. Tucson, Arizona: The University of Arizona Press. pp. 587–624.
- Busemann H., Young A. F., Alexander C. M. O’D., Hoppe P., Mukhopadhyay S., and Nittler L. R. 2006. Interstellar chemistry recorded in organic matter from primitive meteorites. *Science* 312:727–730.
- Busemann H., Zega T. J., Alexander C. M. O’D., Cody G. D., Kilcoyne A. L. D., Nittler L. R., Stroud R. M., and Yabuta H. 2007. Secondary ion mass spectrometry and X-ray absorption near-edge structure spectroscopy of isotopically anomalous organic matter from CR1 chondrite GRO95577 (abstract #1884). 38th Lunar and Planetary Science Conference. CD-ROM.
- Busemann H., Nguyen A. N., Cody G. D., Hoppe P., Kilcoyne A. L. D., Stroud R. M., Zega T. J., and Nittler L. R. 2009. Ultra-primitive interplanetary dust particles from the comet 26P/Grigg-Skjellerup dust stream collection. *Earth and Planetary Science Letters* 288:44–57.
- Busemann H., Alexander C. M. O’D., and Nittler L. R. 2010. Characterization of insoluble organic matter in primitive meteorites by microRaman spectroscopy. *Meteoritics & Planetary Science* 42:1387–1416.
- Chakraborty S., Muskatel B. H., Jackson T. L., Ahmed M., Levine R. D., and Thiemens M. H. 2014. Massive isotopic effect in vacuum UV photodissociation of N<sub>2</sub> and implications for meteorite data. *Proceedings of the National Academy of Sciences* 111:14704–14709.
- Changela H. G., Le Guillou C., Bernard S., and Brearely A. J. 2018. Hydrothermal evolution of the morphology, molecular composition, and distribution of organic matter in CR (Renazzo-type) chondrites. *Meteoritics & Planetary Science* 53:1006–1029.

- Charnley S. B. and Rodgers S. D. 2002. The end of interstellar chemistry as the origin of nitrogen in comets and meteorites. *The Astrophysical Journal Letters* 569: L133.
- Ciesla F. J. and Sandford S. A. 2012. Organic synthesis via irradiation and warming of ice grains in the solar nebula. *Science* 336:452–454.
- Cody G. D. and Alexander C. M. O'D. 2017. The peculiar nature of nitrogen in organic solids from chondritic meteorites (abstract #2747). 48th Lunar and Planetary Science Conference. CD-ROM.
- Cody G. D., Ade H., Alexander C. M. O'D., Araki T., Butterworth A., Fleckenstein H., Flynn G. J., Gilles M. K., Jacobsen C., Kilcoyne A. L. D., Nakamura-Messenger K., Sandford S. A., Tyliszczak T., Westphal A. J., Wirick S., and Yabuta H. 2008. Quantitative organic and light-element analysis of comet 81P/Wild 2 particles using C-, N-, and O- $\mu$ -XANES. *Meteoritics & Planetary Science* 43:353–365.
- Cody G. D., Heying E., Alexander C. M. O'D., Nittler L. R., Kilcoyne A. L. D., Sandford S. A., and Stroud R. M. 2011. Establishing a molecular relationship between chondritic and cometary organic solids. *Proceedings of the National Academy of Sciences* 108:19,171–19,176.
- Collins S. M., Kepaptsoglou D. M., Butler K. T., Longley L., Bennett T. D., Ramasse Q. M., and Midgley P. A. 2019. Subwavelength spatially resolved coordination chemistry of metal-organic framework glass blends. *Journal of the American Chemical Society* 140:17,862–17,866.
- Dartois E., Muñoz Caro G. M., Deboffle D., Montagnac G., and d'Hendecourt L. 2005. Ultraviolet photoproduction of ISM dust. *Astronomy & Astrophysics* 432:895–908.
- De Gregorio B. T., Stroud R. M., Nittler L. R., Alexander C. M. O'D., Kilcoyne A. L. D., and Zega T. J. 2010. Isotopic anomalies in organic nanoglobules from Comet 81P/Wild 2: Comparison to Murchison nanoglobules and isotopic anomalies induced in terrestrial organics by electron irradiation. *Geochimica et Cosmochimica Acta* 74:4454–4470.
- De Gregorio B. T., Stroud R. M., Nittler L. R., Alexander C. M. O'D., Bassim N. D., Cody G. D., Davis A. M., Sandford S. A., Milam S. N., Nuevo M., and Zega T. J. 2013. Isotopic and chemical variation of organic nanoglobules in primitive meteorites. *Meteoritics & Planetary Science* 5:904–928.
- De la Peña F., Fauske V. T., Burdet P., and Prestat E. 2018. hyperspy/hyperspy v1.4.1 (Version v1.4.1). Zenodo. <https://doi.org/10.5281/zenodo.1469364>.
- De Sanctis M. C., Ammannito E., Raponi A., Marchi S., McCord T. B., McSween H. Y., Capaccioni F., Capria M. T., Carozzo F. G., Ciarniello M., Longobardo A., Tosi F., Fonte S., Formisano M., Frigeri A., Giardino M., Magni G., Palomba E., Turrini D., Zambon F., Combe J. P., Feldman W., Jaumann R., McFadden L. A., Pieters C. M., Prettyman T., Toplis M., Raymond C. A., and Russell C. T. 2015. Ammoniated phyllosilicates with a likely outer solar system origin on (1) Ceres. *Nature* 528:241–244.
- Derenne S. and Robert F. 2010. Model of molecular structure of the insoluble organic matter isolated from Murchison meteorite. *Meteoritics & Planetary Science* 45:1461–1475.
- Ehrenfreund P., Rasmussen S., Cleaves J., and Chen L. 2006. Experimentally tracing the key steps in the origin of life: The aromatic world. *Astrobiology* 6:490–520.
- Ferralis N., Matys E. D., Knoll A. H., Hallmann C., and Summons R. E. 2016. Rapid, direct and non-destructive assessment of fossil organic matter via microRaman spectroscopy. *Carbon* 108:440–449.
- Floss C. and Stadermann F. J. 2009. Auger Nanoprobe analysis of presolar ferromagnesian silicate grains from primitive CR chondrites QUE 99177 and MET 00426. *Geochimica et Cosmochimica Acta* 73:2415–2440.
- Floss C., Stadermann F. J., Bradley J., Dai Z. R., Bajt S., and Graham G. 2004. Carbon and nitrogen isotopic anomalies in an anhydrous interplanetary dust particle. *Science* 303:1355–1358.
- Floss C., Stadermann F. J., Bradley J. P., Dai Z. R., Bajt S., Graham G., and Lea A. S. 2006. Identification of isotopically primitive interplanetary dust particles: A NanoSIMS isotopic imaging study. *Geochimica et Cosmochimica Acta* 70:2371–2399.
- Flynn G. J., Keller L. P., Feser M., Wirick S., and Jacobsen C. 2003. The origin of organic matter in the solar system: Evidence from the interplanetary dust particles. *Geochimica et Cosmochimica Acta* 67:4791–4806.
- Füri E. and Marty B. 2015. Nitrogen isotope variations in the solar system. *Nature Geoscience* 8:515–522.
- Garvie L. A. J. and Buseck P. R. 2004. Nanosized carbon-rich grains in carbonaceous chondrite meteorites. *Earth and Planetary Science Letters* 224:431–439.
- Garvie L. A. J. and Buseck P. R. 2006. Carbonaceous materials in the acid residue from the Orgueil carbonaceous chondrite meteorite. *Meteoritics & Planetary Science* 41:633–642.
- Glavin D. P. and Dworkin J. P. 2009. Enrichment of the amino acid L-isovaline by aqueous alteration on CI and CM meteorite parent bodies. *Proceedings of the National Academy of Sciences* 106:5487–5492.
- Goesmann F., Rosenbauer H., Bredehöft J. H., Cabane M., Ehrenfreund P., Gautier T., Giri C., Krüger H., Le Roy L., MacDermott A. J., McKenna-Lawlor S., Meierhenrich U. J., Caro G. M. M., Raulin F., Roll R., Steele A., Steining H., Sternberg R., Szopa C., Thiemann W., and Ulamec S. 2015. Organic compounds on comet 67P/Churyumov-Gerasimenko revealed by COSAC mass spectrometry. *Science* 349, aab0689-1–aab0689-3.
- Hachtel J. A., Huang J., Popovs I., Jansone-Popova S., Keum J. K., Jakowski J., Lovejoy T. C., Dellby N., Krivanek O. L., and Idrobo J. C. 2019. Identification of site-specific isotopic labels by vibrational spectroscopy in the electron microscope. *Science* 363:525–528.
- Hage F. S., Nicholls R. J., Yates J. R., McCulloch D. G., Lovejoy T. C., Dellby N., Krivanek O. L., Refson K., and Ramasse Q. M. 2018. Nanoscale momentum-resolved vibrational spectroscopy. *Science Advances* 4:eaar7495.
- Haiber D. M. and Crozier P. A. 2018. Nanoscale probing of local hydrogen heterogeneity in disordered carbon nitrides with vibrational electron energy loss spectroscopy. *ACS Nano* 12:5463–5472.
- Hashiguchi M., Kobayashi S., and Yurimoto H. 2015. Deuterium- and  $^{15}\text{N}$ -signatures of organic globules in Murchison and Northwest Africa 801 meteorites. *Geochimical Journal* 49:377–391.
- Herd C. D. K., Blinova A., Simkus D. N., Huang Y., Tarozo R., Alexander C. M. O'D., Gyngard F., Nittler L. R., Cody G. D., Fogel M. L., Kebukawa Y., Kilcoyne A. L. D., Hiltz R. W., Slater G. F., Glavin D. P., Dworkin J. P., Callahan M. P., Elsilá J. E., DeGregorio B. T., and



- Stroud R. M. 2011. Origin and evolution of prebiotic organic matter as inferred from the Tagish Lake meteorite. *Science* 332:1304–1307.
- Holzappel C., Soldera F., Vollmer C., Hoppe P., and Mücklich F. 2009. TEM foil preparation of sub-um sized grains by the Focused ion beam technique. *Journal of Electron Microscopy* 235:59–66.
- Hopp T. and Vollmer C. 2017. Chemical composition and iron oxidation state of amorphous matrix silicates in the carbonaceous chondrite Acfer 094. *Meteoritics & Planetary Science* 53:153–166.
- Kebukawa Y., Alexander C. O'D., and Cody G. D. 2011. Compositional diversity in insoluble organic matter in type 1, 2 and 3 chondrites as detected by infrared spectroscopy. *Geochimica et Cosmochimica Acta* 75:3530–3541.
- Kebukawa Y., Kilcoyne A. L. D., and Cody G. D. 2013. Exploring the potential formation of organic solids in chondrites and comets through polymerization of interstellar formaldehyde. *The Astrophysical Journal* 771. <https://doi.org/10.1088/0004-637X/771/1/19>.
- Kebukawa Y., Ito M., Zolensky M. E., Greenwood R. C., Rahman Z., Nakato A., Suga H., Takahashi Y., Takeichi Y., Mase K., Chan Q. H. S., Fries M., and Kobayashi K. 2019. A novel organic-rich meteoritic clast from the outer solar system. *Scientific Reports* 9:3169–3178.
- Keller L. P., Messenger S., Flynn G. J., Clemett S. J., Wirick S., and Jacobsen C. 2004. The nature of molecular cloud material in interplanetary dust. *Geochimica et Cosmochimica Acta* 68:2577–2589.
- King T. V. V., Clark R. N., Calvin W. M., Sherman D. M., and Brown R. H. 1992. Evidence for ammonium-bearing minerals on Ceres. *Science* 255:1551–1553.
- Krivanek O. L., Lovejoy T. C., Dellby N., and Carpenter R. W. 2013. Monochromated STEM with a 30 meV-wide, atom-sized electron probe. *Microscopy* 62:3–21.
- Krivanek O. L., Lovejoy T. C., Dellby N., Aoki T., Carpenter R. W., Rez P., Soignard E., Zhu J., Batson P. E., Lagos M. J., Egerton R. F., and Crozier P. A. 2014. Vibrational spectroscopy in the electron microscope. *Nature* 514:209–212.
- Le Guillou C., Rouzaud J.-N., Bonal L., Quirico E., Derenne S., and Remusat L. 2012. High resolution TEM of chondritic carbonaceous matter: Metamorphic evolution and heterogeneity. *Meteoritics & Planetary Science* 47:345–362.
- Le Guillou C., Bernard S., Brearley A. J., and Remusat L. 2014. Evolution of organic matter in Orgueil, Murchison and Renazzo during parent body aqueous alteration: In situ investigations. *Geochimica et Cosmochimica Acta* 131:368–392.
- Leinweber P., Kruse J., Walley F. L., Gillespie A., Eckhardt K.-U., Blyth R. I. R., and Regier T. 2007. Nitrogen K-edge XANES — An overview of reference compounds used to identify “unknown” organic nitrogen in environmental samples. *Journal of Synchrotron Radiation* 14:500–511.
- Martins Z. 2011. Organic chemistry of carbonaceous meteorites. *Elements* 7:35–40.
- Matrajt G., Messenger S., Brownlee D. E., and Joswiak D. 2012. Diverse forms of primordial organic matter identified in interplanetary dust particles. *Meteoritics & Planetary Science* 47:525–549.
- Muskatell B. H., Remacle F., Thiemens M. H., and Levine R. D. 2011. On the strong and selective isotope effect in the UV excitation of N<sub>2</sub> with implications toward the nebula and Martian atmosphere. *Proceedings of the National Academy of Sciences* 108:6020–6025.
- Nakamura-Messenger K., Messenger S., Keller L. P., Clemett S. J., and Zolensky M. E. 2006. Organic globules in the Tagish Lake meteorite: Remnants of the protosolar disk. *Science* 314:1439–1442.
- Nesvorny D., Jenniskens P., Levison H. F., Bottke W. F., Vokrouhlicky D., and Gounelle M. 2010. Cometary origins of the Zodiacal cloud and carbonaceous micrometeorites. Implications for hot debris disks. *The Astrophysical Journal* 713:816–836.
- Nicholls R. J., Hage F. S., McCulloch D. G., Ramasse Q. M., Refson K., and Yates J. R. 2019. Theory of momentum-resolved phonon spectroscopy in the electron microscope. *Physical Review B* 99:94–105.
- Noguchi T., Yabuta H., Itoh S., Sakamoto N., Mitsunari T., Okubo A., Okazaki R., Nakamura T., Tachibana S., Terada K., Ebihara M., Imae N., Kimura M., and Nagahara H. 2017. Variation of mineralogy and organic material during the early stages of aqueous activity recorded in Antarctic micrometeorites. *Geochimica et Cosmochimica Acta* 208:119–144.
- Peeters Z., Changela H., Stroud R. M., Alexander C. M. O'D., and Nittler L. R. 2012. Organic carbon inclusions in CR2 chondrite Graves Nunataks 95229. *Meteoritics & Planetary Science* 47:A312.
- Pignatelli I., Marrocchi Y., Vacher L. G., Delon R., and Gounelle M. 2016. Multiple precursors of secondary mineralogical assemblages in CM chondrites. *Meteoritics & Planetary Science* 51:785–805.
- Pizzarello S. and Bose M. 2015. The path of reduced nitrogen toward early Earth: The cosmic trail and its solar shortcuts. *The Astrophysical Journal* 814:107–114.
- Pizzarello S. and Shock E. 2017. Carbonaceous chondrite meteorites: The chronicle of a potential evolutionary path between stars and life. *Origins of Life and Evolution of Biospheres* 47:249–260.
- Quirico E., Orthous-Daunay F.-R., Beck P., Bonal L., Brunetto R., Dartois E., Pino T., Montagnac G., Rouzaud J.-N., Engrand C., and Duprat J. 2014. Origin of insoluble organic matter in type 1 and 2 chondrites: New clues, new questions. *Geochimica et Cosmochimica Acta* 136:80–99.
- Saito M. and Kimura Y. 2009. Origin of organic globules in meteorites: Laboratory simulation using aromatic hydrocarbons. *The Astrophysical Journal Letters* 703:L147–L151.
- Schmitt-Kopplin P., Gabelica Z., Gougeon R. D., Fekete A., Kanawati B., Harir M., Gebefuegi I., Eckel G., and Hertkorn N. 2010. High molecular diversity of extraterrestrial organic matter in Murchison meteorite revealed 40 years after its fall. *Proceedings of the National Academy of Sciences* 107:2763–2768.
- Schutte W. A., Allamandola L. J., and Sandford S. A. 1993. An experimental study of the organic molecules produced in cometary and interstellar ice analogs by thermal formaldehyde reactions. *Icarus* 104:118–137.
- Senga R., Suenaga K., Barone P., Morishita S., Mauri F., and Pichler T. 2019. Position and momentum mapping of vibrations in graphene nanostructures. *Nature*. <https://doi.org/10.1038/s41586-019-1477-8>.
- Sephton M. A., Verchovsky A. B., Bland P. A., Gilmour I., Grady M. M., and Wright I. P. 2003. Investigating the variations in carbon and nitrogen isotopes in

- carbonaceous chondrites. *Geochimica et Cosmochimica Acta* 67:2093–2108.
- Simkus D. N., Aponte J. C., Hiltz R. W., Elsila J. E., and Herd C. D. K. 2018. Compound-specific carbon isotope compositions of aldehydes and ketones in the Murchison meteorite. *Meteoritics & Planetary Science* 54:142–156. <https://doi.org/10.1111/maps.13202>.
- Terzieva R. and Herbst E. 2000. The possibility of nitrogen isotopic fractionation in interstellar clouds. *Monthly Notices of the Royal Astronomical Society* 317:563–568.
- Vinogradoff V., Le Guillou C., Bernard S., Binet L., Cartigny P., Brearley A. J., and Remusat L. 2017. Paris vs. Murchison: Impact of hydrothermal alteration on organic matter in CM chondrites. *Geochimica et Cosmochimica Acta* 212:234–252.
- Visser R., Bruderer S., Cazzoletti P., Facchini S., Heays A. N., and Van Dishoeck E. F. 2018. Nitrogen isotope fractionation in protoplanetary disks. *Astronomy and Astrophysics* 615:A75–91.
- Vollmer C., Kepaptsoglou D., Leitner J., Busemann H., Spring N. H., Ramasse Q. M., Hoppe P., and Nittler L. R. 2014. Fluid-induced organic synthesis in the solar nebula recorded in extraterrestrial dust from meteorites. *Proceedings of the National Academy of Sciences* 111:15,338–15,343.
- Wirström E. S., Charnley S. B., Cordiner M. A., and Milam S. N. 2012. Isotopic anomalies in primitive solar system matter: Spin-state-dependent fractionation of nitrogen and deuterium in interstellar clouds. *The Astrophysical Journal* 757:L11–L14.
- Wyckoff S., Tegler S. C., and Engel L. 1991. Nitrogen abundance in comet Halley. *The Astrophysical Journal* 367:641–648.
- Yabuta H., Noguchi T., Itoh S., Nakamura T., Miyake A., Tsujimoto S., Ohashi N., Sakamoto N., Hashiguchi M., Abe K.-I., Okubo A., Kilcoyne A. L. D., Tachibana S., Okazaki R., Terada K., Ebihara M., and Nagahara H. 2017. Formation of an ultracarbonaceous Antarctic micrometeorite through minimal aqueous alteration in a small porous icy body. *Geochimica et Cosmochimica Acta* 214:172–190.
- Zega T. J., Nittler L. R., Busemann H., Hoppe P., and Stroud R. M. 2007. Coordinated isotopic and mineralogic analyses of planetary materials enabled by in situ lift-out with a focused ion beam scanning electron microscope. *Meteoritics & Planetary Science* 42:1373–1386.
- Zega T. J., Alexander C. M. O'D., Busemann H., Nittler L. R., Hoppe P., Stroud R. M., and Young A. F. 2010. Mineral associations and character of isotopically anomalous organic material in the Tagish Lake carbonaceous chondrite. *Geochimica et Cosmochimica Acta* 74:5966–5983.
- Zinner E., Ming T., and Anders E. 1989. Interstellar SiC in the Murchison and Murray meteorites: Isotopic composition of Ne, Xe, Si, C, and N. *Geochimica et Cosmochimica Acta* 53:3273–3290.

## SUPPORTING INFORMATION

Additional supporting information may be found in the online version of this article:

**Table S1.** List of all grains and regions within grains (in *italics*) with heterogeneous compositions detected by NanoSIMS. The N-, and C-isotopic

compositions are given as d-values (deviation from terrestrial standard in per mil), together with the respective  $^{12}\text{C}^{14}\text{N}^-/^{12}\text{C}^-$  ratios. For d $^{15}\text{N}$ -values, we estimate an additional uncertainty of ~15 ‰ due to unknown matrix effects for the organic material. Reported errors in the table are therefore only due to counting statistics and refer to 1s.h